

Creation, storage and retrieval of an optomechanical cat state

R. Y. Teh, S. Kieseewetter

Centre for Quantum and Optical Science, Swinburne University of Technology, Melbourne 3122, Australia

P. D. Drummond and M. D. Reid

*Centre for Quantum and Optical Science, Swinburne University of Technology, Melbourne, Australia and
Institute of Theoretical Atomic, Molecular and Optical Physics,
Harvard University, Cambridge, Massachusetts 02138, USA.*

We analyze a method for the creation, storage and retrieval of optomechanical Schrödinger cat states, in which there is a quantum superposition of two distinct macroscopic states of a mechanical oscillator. In the quantum memory protocol, an optical cat state is first prepared in an optical cavity, then transferred to the mechanical mode, where it is stored and later retrieved using control fields. We carry out numerical simulations for the quantum memory protocol for optomechanical cat states using the positive-P phase space representation. This has a compact, positive representation for a cat state, thus allowing a probabilistic simulation of this highly non-classical quantum system. It is essential to use importance sampling to carry out the simulation effectively. To verify the effectiveness of the cat-state quantum memory, we consider several cat-state signatures and show how they can be computed. We also investigate the effects of decoherence on a cat state by solving the standard master equation for a simplified model analytically, allowing us to compare with the numerical results. Focusing on the negativity of the Wigner function as a signature of the cat state, we evaluate analytically an upper bound on the time taken for the negativity to vanish, for a given temperature of the environment of the mechanical oscillator. We show consistency with the numerical methods. These provide exact solutions, allowing a full treatment of decoherence in an experiment that involves creating, storing and retrieving mechanical cat states using temporally mode-matched input and output pulses. Our analysis treats the internal optical and mechanical modes of an optomechanical oscillator, and the complete set of input and output field modes which become entangled with the internal modes. The model includes decoherence due to thermal effects in the mechanical reservoirs, as well as optical and mechanical losses.

I. INTRODUCTION

Schrödinger's cat [1] features in the investigation of a fundamental issue in quantum mechanics [2–4] namely: Does quantum mechanics hold true in the macroscopic world? This highly nonclassical state is also potentially useful, being proposed as a resource in many quantum information applications including quantum computation [5–7], quantum teleportation [8], quantum metrology [9, 10] and cryptography [11]. As such, there has been much interest in creating Schrödinger cat states of increasing size [12–25]. Recent experiments use superconducting qubits to generate a cat state that is a superposition of two distinguishable coherent states, with the square distance in phase space between the two coherent states up to 80 photons [26] and more recently, 100 photons [27]. It remains a challenge however to prepare a massive, *mechanical* system in a cat state, which has the potential for testing theories of quantum gravity.

As well as being of fundamental importance, there are potential applications. In a proposed quantum internet [28–30], information is transmitted by light in a network of nodes connected by optical fibers. At each node, the quantum information is received and stored, to be later read out or sent to other nodes. A quantum memory [31, 32] is then essential as the information of a quantum state needs to be stored on demand. An optomechanical system is a good candidate for a quantum memory,

where the quantum state is stored in long-lived mechanical modes. In an optomechanical system, the optical and mechanical modes have been demonstrated to interact via radiation pressure in such a way that state transfer between these modes is achievable [33]. In this work, we investigate the storage of a cat state in an optomechanical system. We consider cat states that are a superposition of two distinguishable coherent states.

There have been several earlier proposals to create cat states in mechanical systems. This is a timely goal as quantum control in optomechanics has dramatically improved, notably with the experimental observations of ground state cooling [34–36], quantum state transfer [33, 37] and entanglement generation [26, 38–40] to name a few. In the case of optomechanical cat-state generation, highly nonlinear interactions are typically required. Recently, there are novel schemes to create [41, 42] and enlarge the size of optomechanical cat states [43–45].

Here, we consider an alternative method that involves quantum state transfer from an external optical cavity to the mechanical system, which is essentially utilized as a quantum memory. The type of quantum memory utilized here is an on-demand synchronous dynamical memory, in which the mode-matched input and output of the memory is facilitated by the use of shaped gain and detuning, as treated in previous mode-matched intracavity quantum memory proposals [32, 46]. This general strategy has been previously analyzed for generation of entangled mechanical states [47]. There are related proposals sug-

gested for systems without cavities [48, 49] and some recent strategies in optomechanics of a similar nature, but with different protocols [50, 51].

In our proposal, an optical cat-state is prepared externally, transferred and stored as a mechanical cat-state. It is later retrieved on demand using control fields. An advantage of this method is that optical or microwave cat-states have been generated with high fidelity [15, 27]. The storage time is completely controllable, allowing an analysis of decoherence effects. Finally, the verification measurements can be made externally, using well-developed optical homodyne techniques. This is essential, as there are no current techniques that would allow an *in-situ* quantum state tomography of a mechanical oscillator.

For an efficient quantum memory, the coupling between the input state and the physical system has to be optimized. The system also has to store a quantum state in the desired mode. These goals are achieved with mode matching by choosing an optimal mode function. In Section II, we provide a description of a protocol using mode matching for transferring the cat-state between the optical and mechanical modes. The protocol involves the storage and retrieval of the state, as in a quantum memory. A theoretical model for this protocol was developed earlier [52]. That work however only examined the transfer of a coherent state. The model included dissipation as well as thermal noise.

A cat state is sensitive to fluctuations and noise due to the interaction with its environment. Hence, measurable signatures are needed to verify the presence of a cat state. In Section III, we summarize several quantities that might be used to signify a cat state. These quantities can then be used to give a measure of the effectiveness of the cat-state storage and retrieval. The signatures we examine are the fringe patterns in quadrature probability distributions [41, 42], the Wigner function [16, 26, 27, 53] and its negativity [41, 45], the off-diagonal terms of the density operator [16], and a variance signature [54–62].

We also give an analytical treatment of the decoherence of an idealized cat-state, with detailed calculations of this simplified model in the Appendix, taking into account the thermal occupation number \bar{n}_{th} of the mechanical oscillator reservoir, by solving the standard master equation. The solution tells us how off-diagonal terms decay in time as a function of the cat size, and also provides a way to calculate, for a given value of \bar{n}_{th} , an upper bound on the time for a Wigner function to lose its negativity, which is a typical indicator of non-classicality.

As discussed by Paavola et al. [63], a “sudden death” effect is observed in the presence of thermal noise, which fully converts the cat state to a mixture if the cat state is coupled to the thermal reservoir for long enough time. We report however that the first two signatures undergo a *premature* “sudden death” effect for sufficient coupling time in the absence of thermal noise, failing to indicate non-classicality despite that the cat state has not fully decohered to a mixture of coherent states.

In Section IV the positive-P phase space method used

to solve the full quantum memory model is explained. Despite the highly nonclassical states involved, this can be readily achieved using an exact probabilistic mapping of the full quantum state into a phase-space representation. This involves numerical simulation via the positive-P representation [64], where the dimensionality of the complex phase space is doubled. In this approach the entire input-output process, including all participating optical and mechanical modes as well as dissipation and noise are included, in an exact quantum dynamical simulation. The cat state can be easily treated using this method if an appropriate importance sampling technique is used. This section deals with the methodology for the sampling of the cat-state and its dynamics.

The results of our simulations including predictions for the cat-state signatures and a discussion of feasibility is given in Section V. Here we use typical parameter values from recent electromechanical experiments. We analyze in detail the effects of the different types of decoherence present in the full model. This treats the complete protocol starting from an externally generated cat state, storing it in a mechanical mode, then retrieving and analyzing it externally. As expected, the greater the level of loss and decoherence present, the more quickly the cat signatures are extinguished. We find that cat states with up to 9 mechanical phonons can be stored for short periods with realistic parameter values corresponding to current experiments. This corresponds to a distance metric of $S = |\alpha_1 - \alpha_2|^2 = 36$. Further improvements in temperature and loss rates will be needed to reach $S = 100$, which is the largest cat state generated to date using superconducting waveguide techniques [27]. Results are summarized in Section VI.

II. CAT-STATE TRANSFER

A. Cat-state generation

In electro-optical experiments, cat states have been generated at microwave frequency inside a cavity [27]. We consider the cat state as a quantum superposition of two coherent states $|\alpha_0\rangle$ and $|- \alpha_0\rangle$, in a mode with a corresponding operator $a_0(t)$. This original idealized cat-state has the form

$$|\psi_{cat}\rangle = \frac{1}{\sqrt{\mathcal{N}}} (|\alpha_0\rangle + |-\alpha_0\rangle), \quad (2.1)$$

where the normalizing factor is:

$$\mathcal{N} \equiv 2 \left(1 + \exp \left(-2 |\alpha_0|^2 \right) \right). \quad (2.2)$$

We note that this state will not be completely ideal due to losses and thermal noise, but we assume here that we start with an idealized cat state, in order to analyze the storage and retrieval process.

Having been generated, the state is assumed to be rapidly out-coupled to a waveguide, on time-scales that

are short compared to the originating cavity internal losses and nonlinearities. Following a generic model given in previous work [32, 46, 47], we assume that the output coupler is time-dependent. Using input-output theory, one therefore obtains:

$$\begin{aligned} \frac{d}{dt} a_0(t) &= -\kappa(t) a_0(t) + \sqrt{2\kappa(t)} \hat{\phi}_0^{in} \\ \hat{\phi}_0^{out} &= \sqrt{2\kappa(t)} a_0 - \hat{\phi}_0^{in}. \end{aligned} \quad (2.3)$$

We assume that the state is prepared at time $t = t_0 = -t_W$, then out-coupled at times $t > -t_W$, by turning on the output coupler so that $\kappa(t) > 0$, up until the end of the output process at $t = 0$. The resulting solution for $a_0(t)$ is therefore:

$$a_0(t) = e^{-K(t)} \left[a_0(t_0) + \int_{t_0}^t e^{K(\tau)} \sqrt{2\kappa(\tau)} \hat{\phi}_0^{in}(\tau) d\tau \right], \quad (2.4)$$

where,

$$K(t) = \int_{t_0}^t \kappa(\tau) d\tau \quad (2.5)$$

We choose $K(t)$ and hence $\kappa(\tau)$ so that it corresponds to a precise, temporally mode-matched function $u_0(t)$, where we defube u_0 such that $\hat{\phi}_0^{out}(t) = u_0(t) a_0(t) + \text{noise}$, which implies

$$u_0(t) = \sqrt{2\kappa(t)} \exp\left(-\int_{t_0}^t \kappa(\tau) d\tau\right) \quad (2.6)$$

This requires that $\kappa(\tau)$ obeys the following equation:

$$\frac{d}{dt} \kappa(t) = 2\kappa(t) \frac{d}{dt} \ln u_0(t) + 2\kappa^2(t). \quad (2.7)$$

In general, this is a nonlinear differential equation that requires a numerical solution for any given mode-matching requirement. There are special cases that are analytically soluble, however. One simple case is for a rising exponential mode-function. This is a case that corresponds to the required mode-matched input in the present situation, to a good approximation as described later, with:

$$u_0(t) = \sqrt{2\bar{\gamma}} \exp(\bar{\gamma}t) \Theta(-t). \quad (2.8)$$

Here, $\bar{\gamma}$ is a parameter that sets the time scale of the state transfer protocol as described later. The output coupler solution is then, in the limit of $-\bar{\gamma}t_0 \gg 1$, and for $t < 0$,

$$\kappa(t) = \bar{\gamma} (e^{-2\bar{\gamma}t} - 1)^{-1}. \quad (2.9)$$

This solution is rather simple mathematically. However, it is not the simplest to implement. A one-sided pulse-shape leads to a singular coupling in this approximation, and this appears to be a generic issue related to the sharp temporal cut-off used here in order to have well-defined cat storage times. Yet smooth, two-sided solutions exist as well. These are described in earlier work [46, 47]. The details of this type of mode implementation, and how these change our results, will be given elsewhere.

B. Cat-state download protocol

The approach to optomechanical state transfer used here is based on previous work [52], which we indicate schematically in Fig. 1.

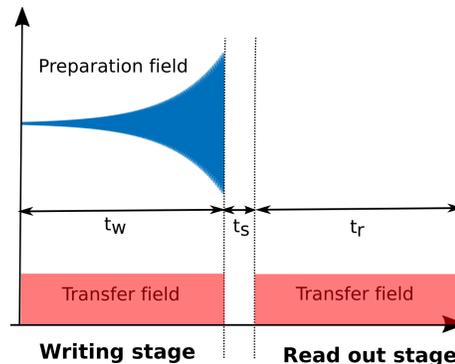


Figure 1. The state transfer protocol. During the writing stage, both the preparation field containing the cat state, and the transfer field that couples the preparation field to the cavity are turned on for a duration of t_w . Both fields are turned off during the storage stage for t_s . The stored state is read out by applying a second transfer field for $t_r = t_w$.

The dynamical protocol for writing the input cat state into the mechanical mode and later retrieving it, requires two pulses at each stage: the preparation and transfer fields. The preparation field is resonant to the optical cavity resonance frequency ω_o , and it prepares the optical cat-state in the cavity. The transfer field, with a frequency ω_d such that the detuning between the cavity and transfer field is the mechanical mode frequency $\Delta = \omega_o - \omega_d = \omega_m$, facilitates the transfer of the cat-state between the optical and mechanical modes. In total, the state transfer protocol consists of three stages, as shown in Fig. 1. The optical quantum state is first generated externally at time $t = t_0 = -t_w$, and transferred to the mechanical state of motion. We note that this process is carried out using a temporal mode-matching protocol to allow efficient transfer, leaving the external source cavity in a vacuum state.

After the successful transfer, both fields are turned off for a time t_s . This allows the system to store the mechanical cat for a prescribed time. This interval needs to be made as long as possible, in order to test decoherence theories. When the quantum state is to be read out, the transfer field is turned on. The stored quantum state is transferred back to an intra-cavity optical mode. Finally, it is coupled out of the cavity with temporal mode-matching to a waveguide traveling mode of duration t_r , for external detection. The protocol is completed at the final time, $t = t_f = t_s + t_r$.

This quantum memory protocol [32, 46] has been experimentally implemented [33] in a superconducting electromechanical device. It is a dynamical scheme which transfers the prepared state from an external source to

the mechanical mode. Temporal mode-matching is used both for input and output. This ensures efficient transfer to and from the external multi-mode waveguide modes. The mechanical state can be coupled out after a well-defined storage time. This procedure allows for studies of time-dependent decoherence.

C. Quantum optomechanical Hamiltonian

A typical optomechanical system consists of an optical cavity and a mechanical oscillator that interact via radiation pressure as shown in Fig. 2. The optics and mechanics are characterized by their resonance frequencies and decay rates. In the single mode model, the optical cavity and mechanical oscillator have resonance frequencies ω_o and ω_m respectively; other frequencies are not involved and can be neglected.

The decay rate of the mechanical oscillator is γ_m while we identify two separate sources of dissipation in the optical cavity: the *internal* and *external* decay rates, γ_{int} and γ_{ext} . The total optical cavity decay rate is $\gamma_o = \gamma_{int} + \gamma_{ext}$. The external cavity decay rate γ_{ext} determines the coupling strength of an input and output field to the cavity, which allows the detection of the cavity optical field. All other sources of dissipation are included in the internal decay rate γ_{int} .

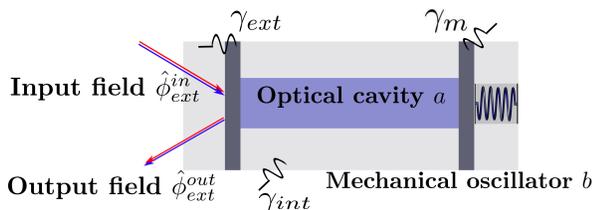


Figure 2. Schematic diagram of the optomechanical system.

The dynamics of an optomechanical system is given by the following standard Hamiltonian [65, 66], in the rotating frame of an external laser field,

$$H = \hbar\Delta a^\dagger a + \hbar\omega_m b^\dagger b + \hbar g_0 a^\dagger a (b + b^\dagger) + \hbar\epsilon(t) (a^\dagger + a), \quad (2.10)$$

where $\Delta = \omega_o - \omega_d$ is the detuning between the cavity resonance frequency ω_o and the external laser carrier frequency ω_d . The third term in Eq. (2.10) corresponds to the nonlinear radiation pressure interaction between the optical and mechanical modes, with a coupling strength determined by g_0 . The mode operators a, b correspond to the intracavity optical and mechanical modes respectively.

The last term includes all external fields $\epsilon(t)$ that are sent into the optical cavity, which includes the external cat state that is imprinted into the system and the transfer field. This is described in greater detail later. In this work, we describe the radiation pressure interaction

term using a simplified, linearized optomechanical Hamiltonian in the interaction picture, where:

$$H_{int} = \hbar g(t) (ab^\dagger + a^\dagger b). \quad (2.11)$$

Here $g(t) = \sqrt{N}g_0 (\Theta(-t) + \Theta(t - t_s))$ is the effective coupling strength and N is the mean photon number in the cavity due to the off-resonant transfer field used for switching [66, 67], Θ is the Heaviside step function, and t_s is the storage time. A rotating wave approximation is used in obtaining the interaction Hamiltonian Eq. (2.11). The linearization approximation is valid when an intense off-resonant driving field is applied to enhance the optomechanical coupling strength, and when the cavity decay rate is much smaller than the mechanical frequency (the resolved sideband regime) [48]. We have investigated the validity of this approximation elsewhere, by carrying out full nonlinear quantum simulations [52, 68].

We treat the optomechanical system as an open quantum system, where the fluctuations of the system due to interactions with its environment are taken into account. This is necessary: a quantum cat-state is fragile and sensitive to perturbations. A standard formalism for treating such an open system is provided by the master equation [69]:

$$\frac{d}{dt}\hat{\rho} = -\frac{i}{\hbar} [H, \hat{\rho}] + \sum_j \gamma_j \left[\bar{n}_j \left(2a_j^\dagger \hat{\rho} a_j - a_j \hat{\rho} a_j^\dagger - \hat{\rho} a_j a_j^\dagger \right) + (\bar{n}_j + 1) \left(2a_j \hat{\rho} a_j^\dagger - a_j^\dagger a_j \hat{\rho} - \hat{\rho} a_j^\dagger a_j \right) \right]. \quad (2.12)$$

Here, $\hat{\rho}$ is the density operator of the optomechanical system, the index $j = 1, 2 \sim o, m$ refer to the cavity and mechanical modes respectively, and \bar{n}_j is the average thermal occupation number from interactions with their corresponding reservoirs.

In our work we extend this approach to include the relevant input and output modes used to create and retrieve the cat state. Owing to its complexity, it is more convenient to solve this large dynamical quantum system using an efficient positive-P phase-space representation. This maps the relevant density matrix into a positive probability distribution, and its dynamics into a numerically tractable set of stochastic equations. We note that while one can integrate the full set of nonlinear equations generated by the full Hamiltonian H , as we have done elsewhere, in this paper we take an idealized case where only the linearized equations obtained from H_{int} are treated.

D. Input-output relations

The state transfer protocol relies on an optimal mode-matching [32, 52] for efficient coupling and detection of both the input and output fields, to and from the optical cavity, respectively. These fields have to be integrated with their corresponding temporal modes $u_{in}(t)$

and $u_{out}(t)$, which are obtained by solving the time evolution equations of the optical a and mechanical b modes.

There are four relevant bosonic mode operators in the model, as well as an infinite set of ‘modes of the universe’ in the input and output channels, giving a total Hilbert space of \mathcal{H} . Apart from selected mode-matched input and output modes, these are optimally maintained in a vacuum state to get the best fidelity, although our method can treat other possibilities, and thermal phonon excitation will be included.

The operator time evolution equations are quantum Langevin equations obtained using the linearized optomechanical Hamiltonian in Eq. (2.11), which are:

$$\begin{aligned} \frac{d}{dt}a(t) &= -\gamma_0 a - ig(t)b + \sqrt{2\gamma_{ext}}\hat{\phi}_{ext}^{in} + \sqrt{2\gamma_{int}}\hat{\phi}_{int}^{in} \\ \frac{d}{dt}b(t) &= -\gamma_m b - ig(t)a + \sqrt{2\gamma_m}\hat{\phi}_m^{in}. \end{aligned} \quad (2.13)$$

The total cavity decay rate is given by $\gamma_0 = \gamma_{ext} + \gamma_{int}$, where γ_{ext} corresponds to output coupling losses through the external mirrors and γ_{int} corresponds to the remaining internal losses in the cavity. The internal fields $\hat{\phi}_{int}^{in}$, $\hat{\phi}_m^{in}$ are the quantum Langevin noise operators due to interaction of the optomechanical system with its internal lossy environment for the photons and mechanical phonons respectively.

The following external input-output relation must also be satisfied:

$$\hat{\phi}_{ext}^{out}(t) = \sqrt{2\gamma_{ext}}a(t) - \hat{\phi}_{ext}^{in}(t), \quad (2.14)$$

where the external input and output fields are traveling waves. These have a mode expansion for the field at the interface mirror given by:

$$\begin{aligned} \hat{\phi}_{ext}^{in}(t) &= \sum_{n \geq 0} a_n^{in} u_n^{in}(t) \\ \hat{\phi}_{ext}^{out}(t) &= \sum_{n \geq 0} a_n^{out} u_n^{out}(t). \end{aligned} \quad (2.15)$$

Here $\hat{\phi}_{ext}^{in}$ is the external input into the cavity, where a_0^{in} is a mode operator for the source of the cat-state, and $a_{n>0}$ is the set of external vacuum mode operators with orthogonal temporal modes given by u_n^{in} . We wish to store the input state of a_0^{in} internally in the optomechanical device, where $u_0^{in}(t)$ is the temporal mode of this preferred input state. This is typically created in a second, external photonic cavity or waveguide [47], and transferred on demand to the quantum memory, with an engineered temporal mode shape. There are many proposals for creating such cat states in the external cavity [70–72], and this choice is left open here. In this work, we assume perfect optomechanical input coupling from the source cavity, so $\hat{\phi}_0^{out}$ in Eq. (2.3) is equal to $\hat{\phi}_{ext}^{in}$ in Eq. (2.15), and u_0 in Eq. (2.6) is equal to u_0^{in} in Eq. (2.3). There is also an output mode $\hat{\phi}_{ext}^{out}(t)$, defined by the the input-output relation [73] given above.

These equations are based on the input-output formalism developed by Gardiner and Collett [73]. Similar treatments of the quantum nature of the optomechanical coupling for the study of entanglement have been given by Hofer et al. [74], He and Reid [75], and Kieseewetter et al. [47, 68].

E. Optimized mode function

Details of the calculations and derivations of these temporal modes can be found in the work of Teh et al. [52]. Here, we note that the solutions of the quantum Langevin equations in Eq. (2.13) are obtained. From these solutions, the optimal temporal mode function $u_0^{in}(t)$ that gives the best mode-matching - in terms of transfer efficiency - is found to be

$$u_0^{in}(t) = -2i \frac{\sqrt{(\gamma_+ + m)(\gamma_+ - m)}\gamma_+}{m} \sinh(mt) e^{\gamma_+ t} \Theta(-t), \quad (2.16)$$

where $\gamma_+ = (\gamma_o + \gamma_m)/2$, $\gamma_- = (\gamma_o - \gamma_m)/2$, $m = \sqrt{\gamma_-^2 - g^2}$, $g = \sqrt{N}g_0$ is the effective optomechanical coupling strength, and Θ is the Heaviside step function. Here we assume that $N(t) = N\Theta(-t)$. The corresponding output temporal mode function $u_0^{out}(t)$ is related to the input temporal mode function $u_0^{in}(t)$ via $u_0^{out}(t) = u_0^{in*}(t_s - t)$, with $N(t) = N\Theta(t - t_s)$.

In particular, the stored mode operator is

$$b(0) = \frac{\sqrt{2\gamma_{ext}}ga_0}{2\sqrt{(\gamma_+ + m)(\gamma_+ - m)}\gamma_+} + \text{noise}. \quad (2.17)$$

From orthonormality of the relevant mode functions, the mode input a_0^{in} and output a_0^{out} containing the fields to be stored and retrieved, respectively, in the optomechanical system are given by:

$$\begin{aligned} a_0^{in} &= \int_{-\infty}^0 u_0^{in*}(t) \hat{\phi}_{ext}^{in}(t) dt \\ a_0^{out} &= \int_{t_s}^{\infty} u_0^{out*}(t) \hat{\phi}_{ext}^{out}(t) dt, \end{aligned} \quad (2.18)$$

where $\hat{\phi}_{ext}^{in}(t)$, $\hat{\phi}_{ext}^{out}(t)$ are the cavity input and output fields. We note that, to a good approximation, if $\gamma_m \ll g \ll \gamma_o$, if $\bar{\gamma} = \gamma_+ - m$, then:

$$u_0^{in}(t) \approx i\sqrt{2\bar{\gamma}}e^{\bar{\gamma}t}\Theta(-t). \quad (2.19)$$

Apart from the phase-factor, which is readily adjustable, this is the approximate exponential form analyzed in treating the download phase from the original cavity. However, we use the full expression in the numerical simulations.

III. CAT-STATE SIGNATURES

As a preliminary exercise, we first consider the signatures of a cat state generated in a single stationary bosonic mode, which is a simplified model of the mechanical mode. The corresponding density operator for the cat state $\hat{\rho}_{cat}$ is then

$$\hat{\rho}_{cat} = \frac{1}{\mathcal{N}} (|\alpha_0\rangle\langle\alpha_0| + |-\alpha_0\rangle\langle-\alpha_0| + |\alpha_0\rangle\langle-\alpha_0| + |-\alpha_0\rangle\langle\alpha_0|). \quad (3.1)$$

It is necessary to verify that the cat state is created and successfully stored in a mechanical mode. This is done by verifying the strength of the cat signature in the retrieved output mode after a storage time t_s . In this paper, three possible cat state signatures are investigated. One of the earliest signatures proposed in the literature is the presence of interference fringes in the quadrature probability density distribution [76]. A second signature is the negativity of the Wigner function, which can be quantified by the negative volume of that Wigner function [77]. As a third signature, we reconstruct the density operator and infer the presence of the optomechanical cat state from the off-diagonal terms [16]. Finally, we discuss a novel variance inequality cat signature, which when violated, implies that the physical state is not in a mixture of two distinguishable coherent states.

A. Interference fringes in quadrature probabilities

Using homodyne detection, the quadrature phase amplitudes can be measured, after the state is transferred to an output photonic mode. The interference fringes in the quadrature probability distribution have been quantified as a cat-measure [41, 42]. Generally, the rotated orthogonal quadratures \hat{X}_θ and $\hat{X}_{\theta+\frac{\pi}{2}}$ are defined in terms of creation and annihilation operators as

$$\begin{aligned} \hat{X}_\theta &= \frac{1}{\sqrt{2}} (e^{-i\theta} a + e^{i\theta} a^\dagger) \\ \hat{X}_{\theta+\frac{\pi}{2}} &\equiv P_\theta = \frac{1}{i\sqrt{2}} (e^{-i\theta} a - e^{i\theta} a^\dagger). \end{aligned} \quad (3.2)$$

The inner product of a coherent state $|\alpha\rangle$ and a rotated quadrature basis state $|x_\theta\rangle$, which is the eigenstate of the quadrature operator \hat{X}_θ and satisfies $\hat{X}_\theta|x_\theta\rangle = x_\theta|x_\theta\rangle$, can be shown to be given by [76]

$$\langle x_\theta|\alpha\rangle = \frac{1}{\pi^{\frac{1}{4}}} \exp\left[-\frac{x_\theta^2}{2} + \sqrt{2}e^{-i\theta}x_\theta\alpha - \frac{e^{-2i\theta}\alpha^2}{2} - \frac{|\alpha|^2}{2}\right], \quad (3.3)$$

with $\alpha = |\alpha|e^{i\phi}$ defined as the complex amplitude of the coherent state $|\alpha\rangle$. In particular, we will consider the case $\theta = 0$, $x_{\theta=0} = x$ and $p_{\theta=0} = x_{\frac{\pi}{2}} = p$. Without losing generality, we also consider a real coherent state amplitude, setting $\phi = 0$.

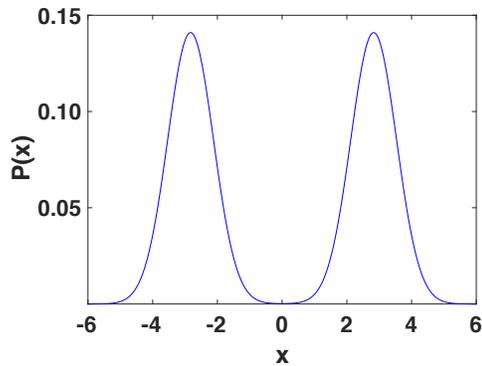


Figure 3. Probability density distribution $P(x)$ for the x quadrature of the cat state Eq. (2.1) with $\alpha_0 = 2$ as given in Eq. (3.4).

The corresponding probability distribution, following Eq. (3.3), is then

$$\begin{aligned} P(x) &= \langle x|\hat{\rho}_{cat}|x\rangle \\ &= \frac{1}{\sqrt{\pi}\mathcal{N}} \left\{ \exp\left[-\left(x - \sqrt{2}\alpha_0\right)^2\right] + \exp\left[-\left(x + \sqrt{2}\alpha_0\right)^2\right] + 2\exp\left[-x^2 - 2\alpha_0^2\right] \right\} \end{aligned} \quad (3.4)$$

for the x quadrature. This distribution, $P(x)$, consists of two exponential terms that correspond to two Gaussian hills around the values $x = \pm\sqrt{2}\alpha_0$, and also a rapidly decaying exponential term, as shown in Fig. 3.

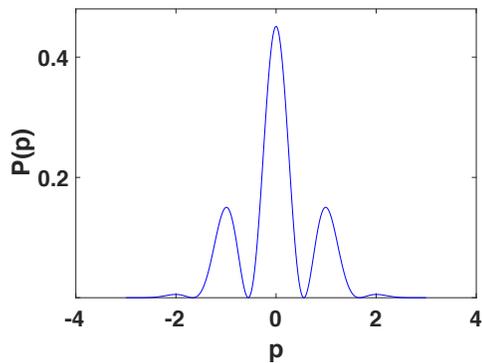


Figure 4. Probability density distributions $P(p)$ for the p quadrature of the cat state Eq. (2.1) with $\alpha_0 = 2$ as given in Eq. (3.5).

On the other hand, the p quadrature probability distribution, $P(p)$, is given by:

$$\begin{aligned} P(p) &= \langle p|\hat{\rho}_{cat}|p\rangle \\ &= \frac{1}{\sqrt{\pi}\mathcal{N}} \left\{ 2\exp(-p^2) \left[1 + \cos\left(2\sqrt{2}p\alpha_0\right) \right] \right\}. \end{aligned} \quad (3.5)$$

This contains a cosine term that gives rise to interference fringes. As shown in Fig. 4, interference fringes arise in the p quadrature probability distribution for the cat-state (2.1). In contrast, for a statistical mixture of two coherent states $|\alpha_0\rangle$ and $|\alpha_0^*\rangle$, the same quantity will show no fringes.

B. Wigner function and Wigner negativity

The Wigner function, introduced by Wigner [78], provides a joint probability distribution $W(x, p)$ of any two conjugate variables x, p for a quantum state. Wigner functions satisfy a set of mathematical properties that one normally associates with a probability distribution [79]. This is certainly true for the marginal distributions. For instance, the marginal distribution for x is given by

$$P(x) = \int_{-\infty}^{\infty} W(x, p) dp \quad (3.6)$$

as for a probability distribution. However, there exist quantum states for which the corresponding Wigner function admits negative values. In this case, the Wigner function cannot be viewed as a probability distribution, but rather is a quasi-probability distribution. The negativity is usually attributed to the non-classicality of the corresponding quantum state.

A cat state is a highly nonclassical physical state that has a Wigner function which admits negative values. In the following, we derive the expression for a cat state Wigner function, which can be obtained from the characteristic function, the Fourier transform of the Wigner function. In particular, we use the Weyl-ordered characteristic function χ_0 :

$$\chi_0(\lambda) = \text{Tr} \left(\hat{\rho}_{cat} e^{\lambda \hat{a}^\dagger - \lambda^* \hat{a}} \right). \quad (3.7)$$

Introducing the complex variable λ , complementary to α , the corresponding Wigner function is then given by

$$W(\alpha) = \int \exp(-\lambda \alpha^* + \lambda^* \alpha) \chi_0(\lambda) \frac{d^2 \lambda}{\pi^2}, \quad (3.8)$$

where we use $\int .. d^2 \lambda$ to indicate an integral over the entire complex plane. For the cat-state density operator in Eq. (3.1), χ_0 consists of four terms and the corresponding Wigner function can be shown to be

$$\begin{aligned} W(\alpha) = \frac{2}{\pi \mathcal{N}} \{ & \exp[-2(\alpha^* - \alpha_0^*)(\alpha - \alpha_0)] \\ & + \exp[-2(\alpha^* + \alpha_0^*)(\alpha + \alpha_0)] \\ & + \langle \alpha_0 | -\alpha_0 \rangle \exp[-2(\alpha^* - \alpha_0^*)(\alpha + \alpha_0)] \\ & + \langle -\alpha_0 | \alpha_0 \rangle \exp[-2(\alpha^* + \alpha_0^*)(\alpha - \alpha_0)] \}. \end{aligned} \quad (3.9)$$

The first two terms correspond to the diagonal terms in the cat-state density operator and are Gaussian distributed, while the last two terms correspond to the off-diagonal terms in the density operator. The Wigner function in Eq. (3.9) for $\alpha_0 = 5$ is plotted in Fig. 5. In terms of experimental measurements, the superposition of α_0 and $-\alpha_0$ corresponds to a squared phase-space distance of $S = |2\alpha_0|^2 = 100$, which has been achieved in superconducting microwave experiments [27].

The two Gaussian peaks arise from the first two terms in Eq. (3.9) while the region that admits negative values comes from the last two terms in Eq. (3.9).

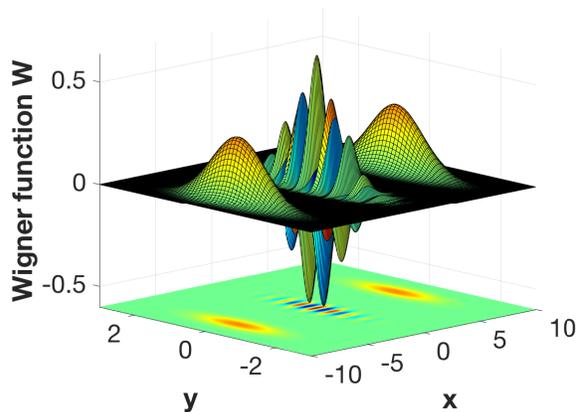


Figure 5. The Wigner function of a cat state as given in Eq. (3.9) for a coherent amplitude $\alpha_0 = 5$. Here, x and y in the plot are the real and imaginary part of α in the Wigner function $W(\alpha)$ respectively.

The Wigner function has been measured in experiments. For instance, the Wigner functions of nonclassical photon states in a cavity are directly measured [53] using the Lutterbach and Davidovich procedure [80]. Using the same procedure, the Wigner function of a two mode cat state is measured more recently [26]. We note that these experiments involve probing the cavity photon state with atoms, which is different from the quantum memory protocol proposed in this paper. To measure quantum states of light, homodyne tomography [81] is needed and this has been carried out both in optomechanical experiments [37, 82] and in experiments that generate optical cat states [43, 83].

Once we have the Wigner function, we can quantify the negativity of the Wigner function by introducing the negative volume δ , which is defined to be [77]

$$\delta = \frac{1}{2} \int [|W(\alpha)| - W(\alpha)] d^2 \alpha. \quad (3.10)$$

A factor of 1/2 in the definition above means that the Wigner negativity δ takes values between 0 and 1, and any value larger than 0 implies that the Wigner function W has negative values.

C. Reconstruction of the density operator

We note that the negativity of a Wigner function is not sufficient to imply the existence of a cat state; it merely signifies the nonclassicality of the state. We get a clearer picture from the presence or absence of the off-diagonal terms in the density operator. In principle, a Wigner function contains all the statistical information about a physical state and hence a density operator can be obtained from a Wigner function. This is done in Section V.

In practice, however, a density operator obtained from an experimentally characterized Wigner function might not be completely positive [84], which is unphysical. This is due to the fact that only a finite number of measurements is recorded in an experiment. Usually, some maximum-likelihood procedure is carried out to find the most likely density operator that characterizes a physical state in an experiment [26, 84].

The modulus of the cat state density operator in the coherent state basis is obtained by

$$|\langle a|\rho_{cat}|b\rangle| = \frac{1}{\mathcal{N}} |(\langle a|\alpha_0\rangle\langle\alpha_0|b\rangle + \langle a|-\alpha_0\rangle\langle-\alpha_0|b\rangle + \langle a|\alpha_0\rangle\langle-\alpha_0|b\rangle + \langle a|-\alpha_0\rangle\langle\alpha_0|b\rangle)|, \quad (3.11)$$

where a , b and α_0 are taken here to be real for simplicity. Fig. 6 shows the modulus of the cat state density operator in the coherent state basis using Eq. (3.11). The presence of off-diagonal terms implies the quantum superposition between the two distinguishable coherent states $|\alpha_0\rangle$ and $|-\alpha_0\rangle$.

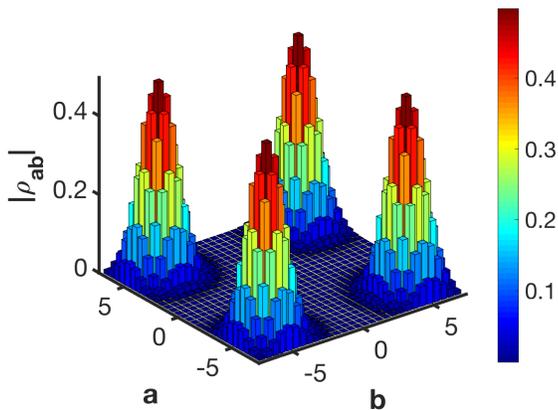


Figure 6. The modulus of the density operator for a cat state in the coherent state basis as given in Eq. (3.11) with coherent amplitude $\alpha_0 = 5$ in the coherent state basis based on Eq. (3.11).

D. Variance method

Alternatively, the cat-state can be distinguished from the mixture $\hat{\rho} = P_+|\alpha_0\rangle\langle\alpha_0| + P_-|-\alpha_0\rangle\langle-\alpha_0|$ by the

method of variances. Variance methods have been used previously to detect quantum coherences [54–62]. If the system is indeed in a mixture of two states $\hat{\rho}_+ = |\alpha_0\rangle\langle\alpha_0|$ and $\hat{\rho}_- = |-\alpha_0\rangle\langle-\alpha_0|$, then it is straightforward to show that the variance in the p quadrature must satisfy

$$(\Delta p)_{mix}^2 \geq \frac{1}{2}. \quad (3.12)$$

This follows by considering that for any mixture $\hat{\rho}_{mix} = \sum_R P_R \hat{\rho}_R$ of states $\hat{\rho}_R$ with probability weightings P_R , the variance $(\Delta p)_{mix}^2$ of the mixture cannot be less than the weighted sum of the variances $(\Delta p)_R^2$ of the components $\hat{\rho}_R$ of the mixture: $(\Delta p)_{mix}^2 \geq \sum_R P_R (\Delta p)_R^2$. Next we use that for all quantum states $\hat{\rho}_R$, $(\Delta x)_R (\Delta p)_R \geq 1/2$, and that for the coherent states $|\alpha_0\rangle$ and $|-\alpha_0\rangle$, it is true that $(\Delta x)_R^2 = \frac{1}{2}$. From this, one can see that for each component of the mixture $(\Delta p)_R^2 \geq \frac{1}{2}$, and the result (3.12) follows.

In fact, the result (3.12) is predicted for *any* mixture $\hat{\rho}_{mix} = P_+ \hat{\rho}_+ + P_- \hat{\rho}_-$ for which the variances of x for $\hat{\rho}_\pm$ are assumed to be respectively $(\Delta x)_\pm^2 \leq \frac{1}{2}$. The experimental observation of $(\Delta p)^2 < 1/2$ in association with the distribution functions shown in Figure 2 thus confirms that the system is not in a mixture of any two states $\hat{\rho}_\pm$, that each generate the Gaussian distributions $P_\pm(x) \sim \exp[-(x \mp \sqrt{2}\alpha_0)^2]$ evident in the $P(x)$.

Calculation of the variance of p for the cat-state (2.1) gives

$$(\Delta p)_{cat}^2 = \frac{1}{2} - \frac{2\alpha_0^2 \exp(-2\alpha_0^2)}{1 + \exp(-2\alpha_0^2)} \quad (3.13)$$

in clear violation of (3.12) for all α_0 . The observation of $(\Delta p)^2 < 1/2$ is a falsification of the mixed state $\hat{\rho}_{mix}$. Even for quite small α_0 , this becomes exceedingly difficult to measure. However, we will see below that there exist regimes of parameter space where $(\Delta p)^2 < 1/2$ for a non-negative Wigner function.

IV. PHASE-SPACE SIMULATIONS

Having identified Schrödinger cat characteristic signatures and expected properties, we now wish to analyze our more realistic optomechanical quantum memory model. This has two relevant coupled modes which can be macroscopically occupied, together with input, output, and reservoir modes. For this, we turn to a more powerful method: the positive-P phase-space representation [64]. This has the advantage that it can readily treat large, entangled Hilbert spaces, together with thermal noise, dissipation, and if necessary nonlinear effects as well [68, 85].

A. Positive-P representation

The master equation given in Eq. (2.12) is an operator equation and is generally intractable, especially if there

is any nonlinearity. Phase space methods can be used to transform this operator equation into a set of stochastic differential equations describing the dynamics of the optical, mechanical and reservoir modes in an optomechanical system. This is achieved by noting that it is always possible to represent the quantum density operator $\hat{\rho}$ as an expansion of a positive probability $P(\vec{\alpha})$ and a set of non-orthogonal projection operators $\hat{\Lambda}(\vec{\alpha})$

$$\hat{\rho} = \int P(\vec{\alpha}) \hat{\Lambda}(\vec{\alpha}) d^2\vec{\alpha}. \quad (4.1)$$

In the general case, $\vec{\alpha} = (\alpha, \alpha^+)$ is a complex vector consisting of two independent complex vectors for each mode, namely $\alpha = (\alpha, \beta, \alpha^{in}, \alpha^{out})$ and $\alpha^+ = (\alpha^+, \beta^+, \alpha^{in+}, \alpha^{out+})$, where α corresponds to an operator vector \mathbf{a} , and α^+ corresponds to \mathbf{a}^\dagger .

Here $\hat{\Lambda}(\vec{\alpha})$ is a set of projection operators parametrized by $\vec{\alpha}$ that forms a complete basis, $P(\vec{\alpha})$ is the corresponding quasi-probability density function, and $d^2\vec{\alpha}$ is an integration measure over the relevant complex space. There are different ways that this can be done, depending on the mapping used. In this paper, the positive-P representation is used, so that the projection operator $\hat{\Lambda}$ is [64]

$$\hat{\Lambda}(\vec{\alpha}) = \frac{|\alpha\rangle\langle\alpha^{+*}|}{\langle\alpha^{+*}|\alpha\rangle} = \prod_m \hat{\Lambda}(\vec{\alpha}_m), \quad (4.2)$$

where $|\alpha\rangle$ is a multimode coherent state [86] and α is the corresponding vector coherent state amplitude, while $\vec{\alpha}_m = (\alpha_m, \alpha_m^+)$ gives the mode amplitude in the m -th mode. This approach generalizes Glauber's P-representation [87], thus allowing the inclusion of non-classical states.

A set of operator identities enables a transformation of the master equation Eq. (2.12) into a Fokker-Planck equation. A probability distribution with a Fokker-Planck equation having positive-definite diffusion always exists in the positive-P representation and hence no truncation approximation is required. The numerical solutions are then exact, apart from the sampling error which can be arbitrarily reduced by increasing the number of samples in a simulation. Possible issues arising from boundary terms, [88] which can be otherwise removed [89], do not appear here. The positive-P representation has the virtue of always being positive, even for quantum states that are highly non-classical, as for instance with cat states. This allows the probabilistic sampling of quantum states. P-functions of this type have been used previously to represent cat states generated dynamically in non-equilibrium parametric oscillators [70–72]. Here we assume that the cat state is already generated, and study how to transfer it to a mechanical oscillator.

B. Stochastic differential equations

From the Fokker-Planck equation, we obtain a corresponding set of stochastic differential equations that describe the time evolution of the cavity α, α^+ and mechanical β, β^+ mode amplitudes. The number of phase space variables is doubled in the positive-P representation where a mode is characterized by two phase space variables in order to represent quantum superpositions. The stochastic differential equations for both the cavity and mechanical mode amplitudes are given by:

$$\begin{aligned} d\alpha &= (-\gamma_o\alpha - ig(t)\beta) dt + d\phi^{in} \\ d\alpha^+ &= (-\gamma_o\alpha^+ + ig(t)\beta^+) dt + d\phi^{in+} \\ d\beta &= (-\gamma_m\beta - ig(t)\alpha) dt + \sqrt{2\gamma_m}d\phi_m^{in} \\ d\beta^+ &= (-\gamma_m\beta^+ + ig(t)\alpha^+) dt + \sqrt{2\gamma_m}d\phi_m^{in+}, \end{aligned} \quad (4.3)$$

where α, α^+ are conjugate in the mean, but not for individual realizations, and

$$\begin{aligned} d\phi^{in} &= \sqrt{2\gamma_{ext}}d\phi_{ext}^{in} + \sqrt{2\gamma_{int}}d\phi_{int}^{in} \\ d\phi_{int}^+ &= \sqrt{2\gamma_{ext}}d(\phi_{ext}^{in})^+ + \sqrt{2\gamma_{int}}d(\phi_{int}^{in})^+. \end{aligned} \quad (4.4)$$

The terms $\phi_{ext}^{in}, \phi_{ext}^{in+}$ are obtained from a mode expansion in terms of external amplitudes $\alpha^{in}, \alpha^{in+}$, as in the operator mode expansion, Eq (2.15), so that:

$$\phi_{ext}^{in}(t) = \sum_{n \geq 0} \alpha_n^{in} u_n^{in}(t) \quad (4.5)$$

The conjugate terms are obtained by the usual mapping of $\phi \rightarrow \phi^+, \alpha \rightarrow \alpha^+$ and $u_n \rightarrow u_n^*$. However, $\phi_m^{in}, \phi_{int}^{in}, \phi_m^{in+}, \phi_{int}^{in+}$ are Langevin noise terms obtained from transforming the master equation (2.12) into a Fokker-Planck equation, using the standard positive-P identities [64].

The effective optomechanical coupling strength $g(t)$ is time dependent due to the optomechanical state transfer protocol used. It is a constant during the writing and readout stages, and zero during the storing stage:

$$g(t) = \begin{cases} \sqrt{N}g_0, & -t_w \leq t \leq 0 \\ 0, & 0 \leq t \leq t_s \\ \sqrt{N}g_0, & t_s \leq t \leq t_r \end{cases}, \quad (4.6)$$

where t_w, t_s , and $t_r = t_w$ are the durations for the writing, storing, and readout stages, respectively, and N is the intra-cavity pump photon number.

The external cavity input $\phi_{ext}^{in}, \phi_{ext}^{in+}$ contain the information about the cat state to be stored in the mode amplitude $\alpha_0^{in}, \alpha_0^{in+}$. Apart from this, the other input modes are assumed to be in vacuum states. The internal cavity $\phi_{int}^{in}, \phi_{int}^{in+}$, and mechanical $\phi_m^{in}, \phi_m^{in+}$ inputs are in thermal equilibrium, and satisfy the following normally ordered correlations:

$$\langle d\phi_i^{in} d\phi_j^{in+} \rangle = \bar{n}_{i,th} \delta_{ij} dt, \quad (4.7)$$

where the indices $i, j = 1, 2 \sim int, m$, and $\bar{n}_{i,th}$ are the mean thermal occupations. In this work, the experimental parameters used mean that only the mechanical thermal bath contributes significantly. The optical thermal noises are neglected.

The input mode into the cavity and output mode from the cavity are related by the input-output relation $\phi_{ext}^{out}(t) = \sqrt{2\gamma_{ext}}\alpha(t) - \phi_{ext}^{in}(t)$ [73], together with a conjugate equation. The integrated output $\alpha_0^{out}, \alpha_0^{out+}$ mode amplitudes can be obtained by integrating these modes with temporal mode functions $u_0^{in}(t)$ and $u_0^{out}(t)$ as given below:

$$\alpha_0^{out} = \int_{t_s}^{\infty} u_0^{out}(t) \phi_{ext}^{out}(t) dt, \quad (4.8)$$

where $u_0^{out}(t)$ is given by a time reversed version of Eq. (2.16), defined for $t > t_s$, and t_s is the storage time. The integrated output mode amplitudes α_0^{out+} are defined similarly.

The input mode function u_0^{in} in Eq. (2.16) has the form $[e^{(\gamma_++m)t} - e^{(\gamma_+-m)t}] \Theta(-t)$, and it can be shown that [52] in the limit where $\gamma_m \ll g \ll \gamma_o$, then $e^{(\gamma_+-m)t} \Theta(-t)$ is the dominating term during the writing stage. This suggests that the duration of the writing stage has to be longer than $1/(\gamma_+ - m)$. However, we use the exact mode-function in our calculations. In this work, we choose the writing stage duration to be $10/(\gamma_+ - m)$. The storage time t_s is chosen to be some fraction of the mechanical lifetime. Finally, the read-out stage has the same duration as the writing stage.

C. Cat state and importance sampling

Initially, we assume that only the external cat state in mode a_0^{in} is excited, so that

$$\hat{\rho} = \hat{\rho}_{cat} \otimes \hat{\rho}', \quad (4.9)$$

where $\hat{\rho}_{cat}$ is the state of the input mode a_0^{in} , and $\hat{\rho}'$ is the state of all the remaining modes, which are assumed to be in the vacuum state, except that the mechanical mode may be initially thermally excited. The cat density operator $\hat{\rho}_{cat}$ in Eq. (3.1) can be expressed in the positive-P representation as follows:

$$\hat{\rho}_{cat} = \int \int P(\vec{\alpha}_0^{in}) \hat{\Lambda}(\vec{\alpha}_0^{in}) d^2\vec{\alpha}_0^{in}. \quad (4.10)$$

One of the possible compact positive-P distributions for the cat state Eq. (2.1) is given by [64, 85]

$$P(\vec{\alpha}_0^{in}) = \frac{1}{\mathcal{N}} \left[\delta_{+,+} + \delta_{-,-} + e^{-2|\alpha_0|^2} (\delta_{+,-} + \delta_{-,+}) \right], \quad (4.11)$$

where $\delta_{\pm,\pm} = \delta(\alpha_0^{in} \pm \alpha_0) \delta(\alpha_0^{in+*} \pm \alpha_0)$. It is straightforward to show that the positive-P distribution in Eq.

(4.11) gives the correct density operator in Eq. (3.1). This distribution is particularly easy to sample. One draws a sample of α_0^{in} and α_0^{in+} with values from one of the possible four terms with the corresponding probability as given in Eq. (4.11).

In order to carry out positive-P simulations, an ensemble of input coherent amplitudes α_0^{in} and α_0^{in+} that corresponds to the correct cat-state statistics has to be sampled from the positive-P distribution in Eq. (4.11). In particular, the last two terms in Eq. (4.11) arise from the off-diagonal terms in the cat-state density operator which is the source of non-classicality in a cat-state.

For the case where α_0 is large, the off-diagonal events are rare in samples taken from the standard positive-P distribution. However, they can have a large effect on some observables. The task is to include these rare, but significant terms in our samples. This is achieved using the importance sampling method, whereby a different distribution is used such that these rare terms are sampled sufficiently. When doing this, both the kernel function $\hat{\Lambda}$ and the probability distribution are modified so as to leave the density operator invariant.

The weighted phase space representation of the input mode density operator is now:

$$\hat{\rho}_{cat} = \int \int f(\vec{\alpha}_0^{in}) \hat{\Lambda}_w(\vec{\alpha}_0^{in}) d^2\vec{\alpha}_0^{in}, \quad (4.12)$$

where $\hat{\Lambda}_w(\vec{\alpha}_0^{in}) \equiv \hat{\Lambda}(\vec{\alpha}_0^{in}) w(\vec{\alpha}_0^{in})$ is the weighted kernel function with weight $w(\vec{\alpha}_0^{in}) = P(\vec{\alpha}_0^{in})/f(\vec{\alpha}_0^{in})$, associated with the sampling of the distribution $f(\vec{\alpha}_0^{in})$. A natural initial distribution choice is a probability distribution of the form $f(\vec{\alpha}_0^{in}) = \frac{1}{4}(\delta_{+,+} + \delta_{-,-} + \delta_{+,-} + \delta_{-,+})$, with equal probability assigned to each term. Instead of representing the cat-state density operator $\hat{\rho}_{cat}$ in terms of projection operators $|\alpha_0^{in}\rangle\langle\alpha_0^{in+*}|/|\langle\alpha_0^{in+*}|\alpha_0^{in}\rangle|$ with the corresponding probability distribution $P(\vec{\alpha}_0^{in})$, it is now expressed in terms of an operator $\hat{\Lambda}_w(\vec{\alpha}_0^{in})$, with the new probability distribution $f(\vec{\alpha}_0^{in})$. This weight function has to be taken into account when we compute any observables.

The *total* initial density operator can now be written as:

$$\hat{\rho}_0 = \int F_0(\vec{\alpha}) \hat{\Lambda}_w(\vec{\alpha}) d^2\vec{\alpha}. \quad (4.13)$$

Here $\hat{\Lambda}_w(\vec{\alpha}) \equiv \hat{\Lambda}(\vec{\alpha}) w(\vec{\alpha}_0^{in})$ and $F_0(\vec{\alpha}) = f(\vec{\alpha}_0^{in}) P'(\vec{\alpha}')$, where $\vec{\alpha}'$ represents the other modes of the system, initially in a vacuum or thermal state described by the distribution $P'(\vec{\alpha}')$. With this new quasi-probability distribution, $F_0(\vec{\alpha})$, any moments we compute have to be weighted according to $w(\vec{\alpha}_0^{in})$ to obtain correct results. This is because $\hat{\Lambda}_w(\vec{\alpha})$ no longer has a unit trace, and in fact for any trace that includes the weighted input mode,

$$tr[\hat{\Lambda}_w(\vec{\alpha})] = w(\vec{\alpha}_0^{in}). \quad (4.14)$$

We also note that, somewhat counter-intuitively, the input mode amplitudes $\vec{\alpha}_0^{in}$ are time-invariant. This is because, in simple terms, they have a 'use-by' time. The effect of these mode amplitudes is transmitted to the cavity through the associated time-dependent mode-function $u_0(t)$, rather than through any change in the input amplitudes themselves.

D. Wigner function and interference fringes

In this subsection, we describe how a cat signature can be computed numerically. The simplest cat signature is an interference fringe, obtained from homodyne measurements on the output field. This is directly computable from the density operator, and hence one can obtain a sampled representation of interference by summing over the stochastic trajectories. We note that the total density operator $\hat{\rho}$ is a multimode operator, while the cat signatures are inferred only from the integrated output modes. To this end, we define a projection operator $|p\rangle\langle p|$ that only acts on the chosen output mode. To evaluate this, it is simple to trace over the non-observed modes, thus generating a single-mode density matrix, now defined in terms of the output mode amplitudes $\vec{\alpha}_0^{out}$. These amplitudes are evaluated through the integrals of Eq (4.8).

We define the output single-mode density matrix as a partial trace of the density matrix over all modes *except* the mode-matched output mode, at the final evolution time of the density matrix:

$$\hat{\rho}_{out} = \text{tr}_{\mathcal{H}'} [\hat{\rho}(t = t_f)]. \quad (4.15)$$

This has a phase-space representation of:

$$\hat{\rho}_{out} = \int P(\vec{\alpha}_0^{out} | \vec{\alpha}_0^{in}) w(\vec{\alpha}_0^{in}) \hat{\Lambda}(\vec{\alpha}_0^{out}) d\vec{\alpha}_0^{out} d\vec{\alpha}_0^{in}. \quad (4.16)$$

Here, $P(\vec{\alpha}_0^{out} | \vec{\alpha}_0^{in})$ is the conditional probability of observing $\vec{\alpha}_0^{out}$ given an input amplitude $\vec{\alpha}_0^{in}$, and it is obtained by integrating the P-distribution over all the unobserved modes except the input and output modes. The output quadrature probability distribution can then be computed as follows:

$$\begin{aligned} P(p) &= \text{Tr}[\hat{\rho}_{out}|p\rangle\langle p|] \\ &= \int P(\vec{\alpha}_0^{out} | \vec{\alpha}_0^{in}) w(\vec{\alpha}_0^{in}) \text{Tr}(\hat{\Lambda}(\vec{\alpha}_0^{out}) |p\rangle\langle p|) d\vec{\alpha}_0^{out} d\vec{\alpha}_0^{in} \end{aligned} \quad (4.17)$$

The output mode is traced out in the second line of Eq. (4.17).

We compute the probability distribution $P(p)$ of the integrated output modes α_0^{out} , α_0^{out+} to verify the presence of cat state in the quantum memory. In the Monte Carlo method, $P(p)$ in Eq. (4.17) is estimated from N_s phase-space samples, $[\vec{\alpha}_1, \dots, \vec{\alpha}_{N_s}]$. This is shown explic-

itly below:

$$P(p) \approx \frac{1}{N_s} \sum_{i=1}^{N_s} w(\vec{\alpha}_{0,i}^{in}) \frac{\langle p | \alpha_{0,i}^{out} \rangle \langle \alpha_{0,i}^{out+*} | p \rangle}{\langle \alpha_{0,i}^{out+*} | \alpha_{0,i}^{out} \rangle}. \quad (4.18)$$

In particular, samples with index i going from 1 to $N_s/2$ correspond to diagonal terms in the density operator and they have a weight function $w = 2 / (1 + e^{-2|\alpha_0|^2})$, while samples with index i going from $N_s/2 + 1$ to N_s correspond to off-diagonal terms in the density operator and the weight function is $w = 2e^{-2|\alpha_0|^2} / (1 + e^{-2|\alpha_0|^2})$. For cases where the mechanical thermal noise $\bar{n}_{th} \neq 0$, the accuracy of the estimation improves with the number of samples N_s . At zero temperature there is no sampling error, giving an extremely efficient procedure.

In order to obtain the Wigner function of the integrated output modes, it is necessary to relate the positive-P function to its corresponding Wigner function. We write down the expression of the Wigner function in terms of the symmetrical-ordered characteristic function and then represent the density operator $\hat{\rho}_{out}$ in that characteristic function in the positive-P representation. These steps are explicitly shown below:

$$\begin{aligned} W(\alpha) &= \frac{1}{\pi^2} \int e^{(-\lambda\alpha^* + \lambda^*\alpha)} \chi_W(\lambda) d^2\lambda \\ &= \frac{2}{\pi} \int P(\vec{\alpha}_0^{out} | \vec{\alpha}_0^{in}) w(\vec{\alpha}_0^{in}) e^{[-2(\alpha_0^{out+} - \alpha^*)(\alpha_0^{out} - \alpha)]} d\vec{\alpha}_0^{out} d\vec{\alpha}_0^{in} \end{aligned} \quad (4.19)$$

In going from line 1 to line 2 in Eq. (4.19), the characteristic function $\chi_W(\lambda) = \text{Tr}(\hat{\rho}_0^{out} e^{\lambda\hat{a}^\dagger - \lambda^*\hat{a}})$ is used, and the density operator $\hat{\rho}_{out}$ is expressed in the positive-P representation as previously mentioned. Eq. (4.19) is then computed numerically for the integrated output modes α_0^{out} , α_0^{out+} using the Monte Carlo method, giving:

$$W(\alpha) \approx \frac{2}{\pi N_s} \sum_i^{N_s} w(\vec{\alpha}_{0,i}^{in}) e^{[-2(\alpha_{0,i}^{out+} - \alpha^*)(\alpha_{0,i}^{out} - \alpha)]}. \quad (4.20)$$

Here, the weight function w is identical to the one given in Eq. (4.18).

V. NUMERICAL RESULTS

In this section, we describe the numerical method and results for the cat-state signatures discussed in Section III. In all of the simulations carried out, both the cavity and mechanical modes are initially in their ground or thermally excited states. The cat state is then sent into the cavity, where the cat state is sampled using the importance sampling method discussed in the previous section. We generate four different types of positive-P

trajectories which correspond to two diagonal terms and two off-diagonal terms in the cat state density operator. All numerical simulations were carried out in the positive-P representation.

A. Parameter values

Going through the quantum memory protocol as described in Section II B, the output from the cavity is subsequently integrated to give the output mode amplitudes $\vec{\alpha}_0^{out} = (\alpha_0^{out}, \alpha_0^{out+})$ in Eq. (4.8). These output modes are the quantum states stored in the quantum memory and all cat state signatures computed in this section are based on these output modes amplitudes.

For definiteness, we use experimental parameters from the electromechanical experiment of Palomaki et al. [33]. In their experiment, the resonator and mechanical decay rates are $\gamma_o/2\pi = 170\text{kHz}$ and $\gamma_m/2\pi = 17.5\text{Hz}$ respectively, and the bare electromechanical coupling strength g_0 is $2\pi \times 200\text{Hz}$.

All numerical simulations are carried out using xSPDE, which is a Matlab open software package designed specially for solving stochastic differential equations [90]. The algorithm used for solving the stochastic differential equations is the fourth-order Runge-Kutta method in the interaction picture [90, 91]. As the linearized optomechanical Hamiltonian is used for this work, the highest frequency parameter in the stochastic differential equations is the decay rate γ_o . Based on the Shannon sampling theorem [92], we choose a time step, $\Delta t = 1/(10\gamma_o)$ that is smaller than the sufficient sampling rate criterion, which predicts that a time step less than $1/(2\gamma_o)$ is needed.

We express all stochastic differential equations in dimensionless form, using a dimensionless time variable $\tau = \gamma_o t$ where γ_o is the resonator decay rate. All parameters then have values that are relative to the resonator decay rate γ_o . These dimensionless parameters are denoted by capitalizing the Greek letters of their corresponding experimental parameters. We choose the dimensionless effective optomechanical coupling strength $G = g/\gamma_o = 0.6$. This places the optomechanical system in the weak coupling regime, where the linearization approximation is valid [52]. We take the initial optical and mechanical states to be in their ground state, except in the last case treated. In simulations where the mechanical thermal noise $\bar{n}_{th} = 0$, we take a total of four samples, which corresponds to four different trajectories for two diagonal and two off-diagonal terms in the density operator. In cases where $\bar{n}_{th} \neq 0$, a total number of 2×10^5 samples are taken.

B. Interference fringes

Using the method of Eq (4.18), fringes were calculated for a cat state with amplitude $\alpha_0 = 5$ corresponding to

25 stored phonons. In Fig. 7, we plot the p -quadrature distribution after the readout from the optomechanical quantum memory. In this figure, there is no internal cavity loss and the storage time is $0.02/\Gamma_m$.

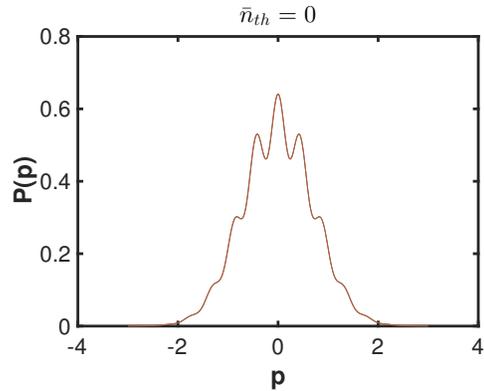


Figure 7. The p -quadrature probability distribution computed using the positive-P distribution with Eq. (4.18) for $\alpha_0 = 5$ after reading out from the quantum memory. The mean mechanical thermal noise and internal loss rate are chosen to be $\bar{n}_{th} = \Gamma_{int} = 0$ throughout the simulation. Here, the optomechanical cat state has a low decoherence due to the short storage time compared to the mechanical oscillator lifetime. This figure is for a storage time of $0.02/\Gamma_m$. A total number of 4 samples are taken.

The same quantity but with a storage time $0.3466/\Gamma_m$ is shown in Fig. 8. This storage time corresponds to the time a Wigner function loses its negativity for a mean mechanical thermal number $\bar{n}_{th} = 0$ as given by Eq. (6.12). We note in this case, the fringe pattern has vanished, consistent with a loss of non-classicality.

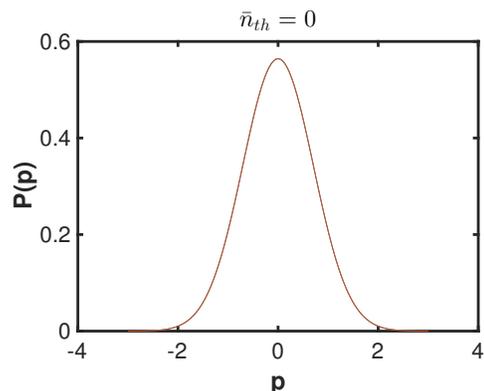


Figure 8. The p -quadrature probability distribution computed using the positive-P distribution with Eq. (4.18) for $\alpha_0 = 5$. Other parameters as in Fig (7). Here, the optomechanical cat state decoheres for a storage time of $0.3466/\Gamma_m$, which is the time a Wigner function loses its negativity according to Eq. (6.12).

C. Wigner function

The Wigner function and its projection onto the phase space plane are plotted in Fig. 9 and Fig. 10 for storage times $0.02/\Gamma_m, 0.3466/\Gamma_m$ respectively. The storage time $0.3466/\Gamma_m$ corresponds to the time a Wigner function loses its negativity for a mean mechanical thermal number $\bar{n}_{th} = 0$ as given by Eq. (6.12).

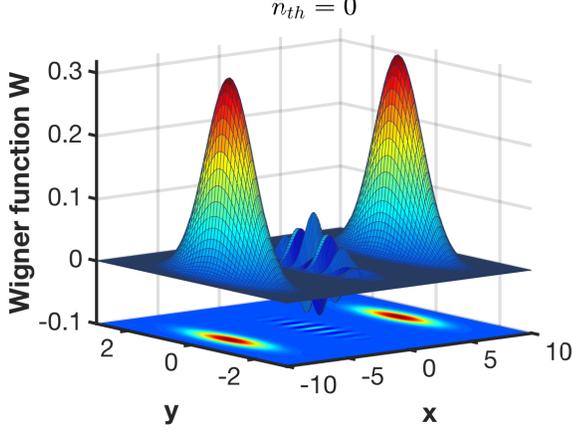


Figure 9. The Wigner function computed using the positive-P distribution and Eq. (4.20) for $\alpha_0 = 5$ after reading out from the quantum memory. Here, x and y in the plot are the real and imaginary part of α in the Wigner function $W(\alpha)$ in Eq. (4.20) respectively. Other parameters as in Fig (7). This figure has a storage time of $0.02/\Gamma_m$, too short for substantial decoherence.

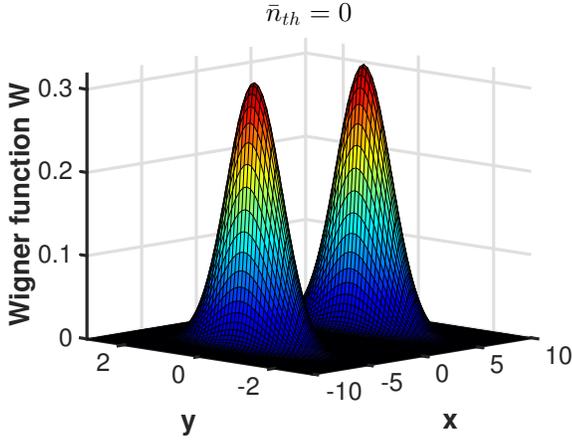


Figure 10. The Wigner function computed using the positive-P distribution and Eq. (4.20) for $\alpha_0 = 5$ after reading out from the quantum memory. As previously, x and y in the plot are the real and imaginary part of α in the Wigner function $W(\alpha)$ in Eq. (4.20) respectively. Other parameters as in Fig (8). Here, the optomechanical cat state decoheres after a storage time of $0.3466/\Gamma_m$, which is the time a Wigner function loses its negativity according to Eq. (6.12).

D. Reconstructed density operator

We reconstruct the density operator by looking at the modulus of the density operator in the coherent state basis: $|\rho_{ab}| = |\langle a|\hat{\rho}_0^{out}|b\rangle|$. This can be achieved using the Monte Carlo method as discussed in the previous section and is shown below:

$$|\rho_{ab}| = |\langle a|\hat{\rho}_0^{out}|b\rangle| \approx \left| \frac{1}{N_s} \sum_i^{N_s} w(\bar{\alpha}_{0,i}^{in}) \frac{\langle a|\alpha_{0,i}^{out}\rangle \langle \alpha_{0,i}^{out+*}|b\rangle}{\langle \alpha_{0,i}^{out+*}|\alpha_{0,i}^{out}\rangle} \right|. \quad (5.1)$$

Here, the weight function w is identical to the one given in Eq. (4.18). The reconstructed density operator in the coherent state basis is plotted in Fig. 11 and Fig. 12 for storage times $0.02/\Gamma_m, 0.3466/\Gamma_m$ respectively. The storage time $0.3466/\Gamma_m$ corresponds to the time a Wigner function loses its negativity for a mean mechanical thermal number $\bar{n}_{th} = 0$ as given by Eq. (6.12). Here we note the presence of the nonzero off-diagonal terms, for times where the Wigner negativity is zero.

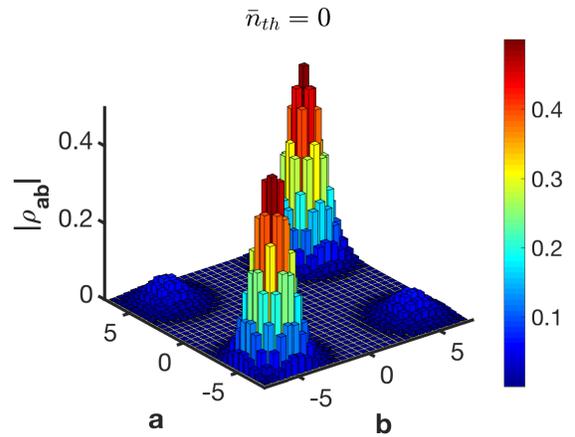


Figure 11. The reconstructed density operator computed using the positive-P distribution and Eq. (5.1) for $\alpha_0 = 5$ after reading out from the quantum memory. The mean mechanical thermal noise and internal loss rate are chosen to be $\bar{n}_{th} = \Gamma_{int} = 0$, and the storage time is $0.02/\Gamma_m$. A total number of 4 samples are taken.

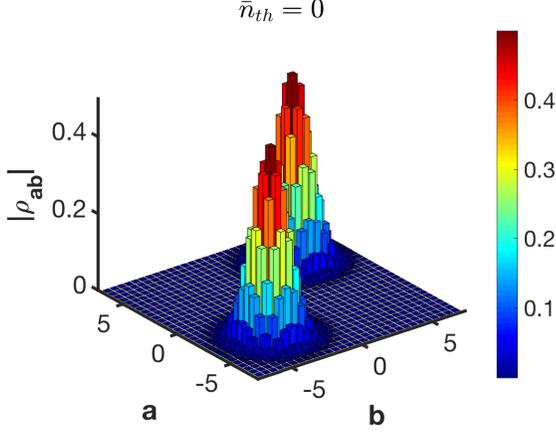


Figure 12. The reconstructed density operator computed using the positive-P distribution and Eq. (5.1) for $\alpha_0 = 5$ after reading out from the quantum memory. The mean mechanical thermal noise and internal loss rate are chosen to be $\bar{n}_{th} = \Gamma_{int} = 0$. Here, the optomechanical cat state decoheres due to the finite mechanical lifetime after a storage time of $0.3466/\Gamma_m$, which is the time a Wigner function loses its negativity according to Eq. (6.12). A total number of 4 samples are taken.

E. Wigner negativity

We also compute the Wigner negativity as defined in Eq. (3.10) as a function of the optomechanical cat storage time and thermal noise. The Wigner negativity can be easily computed numerically once the Wigner function has been obtained, and we use the trapezoidal numerical method to carry out the integration involved.

The numerical results are then compared with the corresponding analytical results based on the idealized characteristic function solution in Eq. (6.7). We define an auxiliary amplitude given by

$$\alpha_{\pm}(t) = \alpha \pm \alpha_0 e^{-\Gamma_m t}. \quad (5.2)$$

The Wigner function at time t as a function of cat state amplitude, storage time and mean mechanical thermal number is given by

$$\begin{aligned} W(\alpha, t) = & \frac{2}{\pi \mathcal{N}} \frac{1}{1 + 2\bar{n}_{th}(1 - e^{-2\Gamma_m t})} \times \\ & \left\{ \exp \left[-\frac{2\alpha_-^*(t)\alpha_-(t)}{1 + 2\bar{n}_{th}(1 - e^{-2\Gamma_m t})} \right] \right. \\ & + \exp \left[-\frac{2\alpha_+^*(t)\alpha_+(t)}{1 + 2\bar{n}_{th}(1 - e^{-2\Gamma_m t})} \right] \\ & + \langle \alpha_0 | -\alpha_0 \rangle \exp \left[-\frac{2\alpha_-^*(t)\alpha_+(t)}{1 + 2\bar{n}_{th}(1 - e^{-2\Gamma_m t})} \right] \\ & \left. + \langle -\alpha_0 | \alpha_0 \rangle \exp \left[-\frac{2\alpha_+^*(t)\alpha_-(t)}{1 + 2\bar{n}_{th}(1 - e^{-2\Gamma_m t})} \right] \right\}. \quad (5.3) \end{aligned}$$

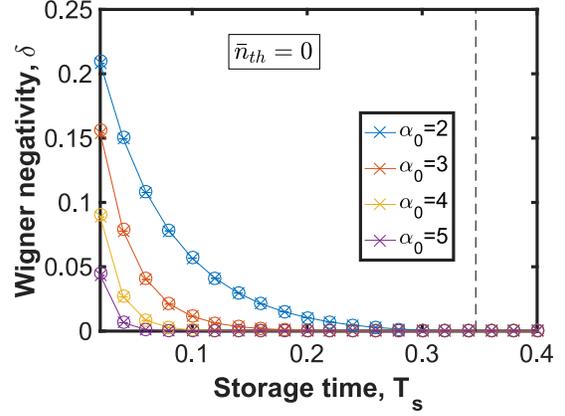


Figure 13. The Wigner negativity of the read-out state as a function of the dimensionless storage time (in multiples of $1/\Gamma_m$) for cat amplitudes $\alpha_0 = 2, 3, 4$ and 5 . The mean mechanical thermal occupation number and internal loss rate are chosen to be $\bar{n}_{th} = \Gamma_{int} = 0$. The corresponding data points in circles are analytical values based on Eq. (5.3). The dashed vertical line is the upper bound of the time for a Wigner function to lose its negativity, as given in Eq. (6.12). For $\bar{n}_{th} = 0$, the upper bound, in multiples of $1/\Gamma_m$, is 0.3466 . A total number of 4 samples are taken. The error bars denote the time-step error in the phase-space simulations.

The Wigner negativity from both the analytical and numerical methods are plotted in Fig. 13 and Fig. 14 for a mean mechanical thermal occupation number \bar{n}_{th} of 0 and 2, respectively. Fig. 15 shows a three-dimensional representation of the Wigner negativity results as a function of mean mechanical thermal occupation number and storage time.

F. Variance of the p -quadrature

Here, we compute the variance of p -quadrature before the cat-state is stored and after the state has been read out from the quantum memory. In particular, we compute this observable for storage times where the corresponding Wigner functions for the quantum memory output states lose their negativity, with zero mean mechanical thermal number. Note that the positive-P representation computes normally ordered observables. Hence, a quantity such as $\langle \hat{p}^2 \rangle$ has to be normally ordered first for the numerical results in the positive-P representation to be correct. Thus

$$\begin{aligned} \langle \hat{p}^2 \rangle &= -\frac{1}{2} (\langle \hat{a}^2 \rangle + \langle \hat{a}^{\dagger 2} \rangle - 2\langle \hat{a}^\dagger \hat{a} \rangle - 1) \\ &= -\frac{1}{2} (\langle \alpha^2 \rangle_p + \langle \alpha^{+2} \rangle_p - 2\langle \alpha^\dagger \alpha \rangle_p - 1), \quad (5.4) \end{aligned}$$

where α, α^+ are the complex field amplitudes in the positive-P representation. We compare the numerical results for the variance with the corresponding analytical ones as given by Eq. (3.13). The comparison is shown in Table I.

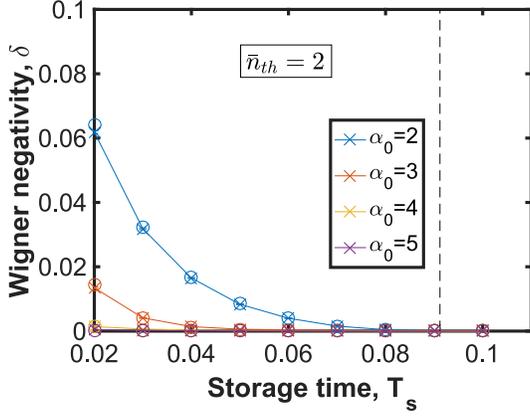


Figure 14. The Wigner negativity of the read-out state as a function of the dimensionless storage time (in multiples of $1/\Gamma_m$) for cat amplitudes $\alpha_0 = 2, 3, 4$ and 5 . The mean mechanical thermal occupation number $\bar{n}_{th} = 2$, and the internal loss is $\Gamma_{int} = 0$. The dashed vertical line is the upper bound of the time for a Wigner function to lose its negativity, as given in Eq. (6.12). For $\bar{n}_{th} = 2$, the upper bound, in multiples of $1/\Gamma_m$, is 0.0912 . A total number of 2×10^5 samples are taken. The error bars include both the sampling error and time-step error.

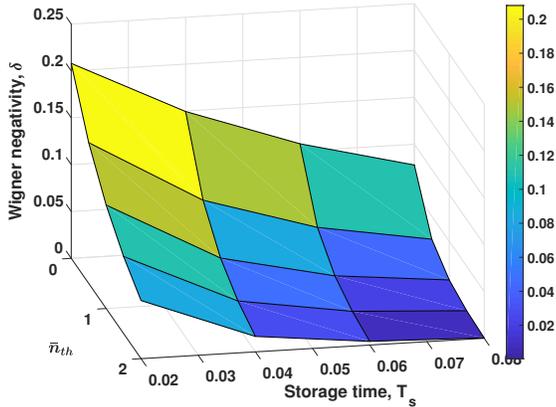


Figure 15. The Wigner negativity of the read-out state as a function of the dimensionless storage time, T_s (in multiples of $1/\Gamma_m$) and the mean mechanical thermal number \bar{n}_{th} for a cat amplitude $\alpha_0 = 2$. The internal loss is $\Gamma_{int} = 0$. A total number of 2×10^5 samples are taken, except when $\bar{n}_{th} = 0$, where 4 samples are taken instead.

Cat amplitude, α_0	Analytical prediction for a cat state, $(\Delta p)_{cat}^2$	Numerical value before storage, $(\Delta p)_{in}^2$	Numerical value after readout, $(\Delta p)_{out}^2$
1	0.2616	0.2616	0.3809
2	0.4973	0.4973	0.4987
3	0.5000	0.5000	0.5000
5	0.5000	0.5000	0.5000

Table I. The analytical and numerical values for the variance of p -quadrature for different cat amplitudes α_0 . The analytical values are obtained using the expression in Eq. (3.13). These values are obtained for the parameters $\bar{n}_{th} = 0$ and a storage time of $1/2\ln(2)$, which is the upper bound time for the loss of Wigner negativity of the readout state.

In practice, the variance of p -quadrature for a cat state is too tiny to be differentiated from the variance of p -quadrature for a mixed state, for a cat state amplitude larger than 2. However, in the cases where $(\Delta p)^2 < 1/2$ can be observed, the variance method serves as a sufficient criterion to verify the existence of a cat state. This is crucial as we see that for $\bar{n}_{th} = 0$ and a storage time that corresponds to a state where its Wigner function loses its negativity, only the reconstructed density operator and the variance methods are able to detect the presence of a density operator with non-vanishing off-diagonal terms. The variance method has the advantage that no state tomography is needed, as opposed to the density operator reconstructed approach.

G. Decoherence effects on an optomechanical cat state

In the previous subsection, the internal cavity decay rate is set to zero, which corresponds to an optimal optomechanical quantum state transfer. In practice, the internal cavity decay rate is nonzero, causing the quantum state transfer to be less efficient. This introduces further decoherence to the quantum state that is stored. In this section, we analyze more realistic parameter values that correspond to recent electromechanical experiments.

First we consider the case where there is a nonzero optical internal loss, Γ_{int} . The state transfer protocol used in this paper predicts that the stored amplitude, given an initial coherent amplitude α , would have an expectation value of

$$\langle b(0) \rangle = \frac{\sqrt{2\Gamma_{ext}}G\alpha}{2\sqrt{(K_+ + M)(K_+ - M)K_+}}, \quad (5.5)$$

based on Eq. (2.17). If we consider a realistic internal cavity decay rate $\Gamma_{int} = 0.05$, then from the set of parameters we use, the stored amplitude is 0.9745α . As shown in Fig. 16, this significantly reduces the Wigner negativity of the retrieved cat state, even at zero temperature.

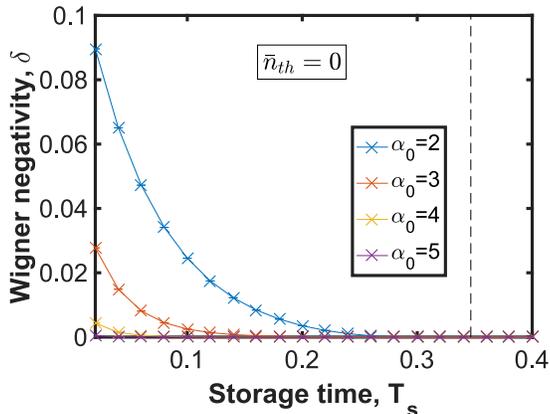


Figure 16. The Wigner negativity of the read-out state as a function of the dimensionless storage time (in multiples of $1/\Gamma_m$) for cat amplitudes $\alpha_0 = 2, 3, 4$ and 5 . The mean mechanical thermal occupation number $\bar{n}_{th} = 0$. The internal cavity decay rate is nonzero and contributes to further decoherence of the cat state. Here, the internal cavity decay rate is set to be $\Gamma_{int} = 0.05$. A total number of 4 samples are taken. The error bars denote the time-step error in the phase-space simulations.

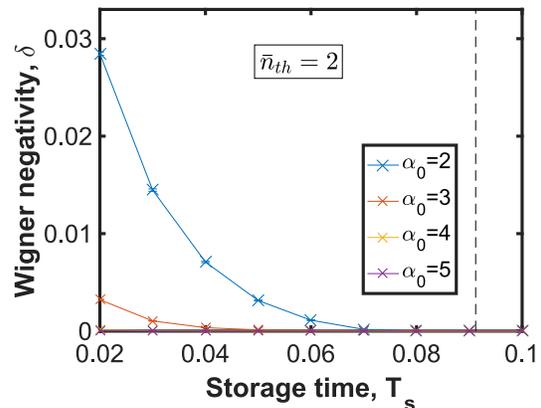


Figure 17. The Wigner negativity of the read-out state as a function of the dimensionless storage time (in multiples of $1/\Gamma_m$) for cat amplitudes $\alpha_0 = 2, 3, 4$ and 5 . The mean mechanical thermal occupation number $\bar{n}_{th} = 2$. The internal cavity decay rate is nonzero and contributes to further decoherence of the cat state. Here, the internal cavity decay rate is set to be $\Gamma_{int} = 0.05$ and the initial mechanical mode has an occupation number of 0.5 . A total number of 2×10^5 samples are taken. The error bars include both the sampling error and time-step error.

Next, we consider the effect of finite thermal occupation numbers in the mechanical mode. In Fig. 17, we show the result for the Wigner negativity for internal cavity decay rate $\Gamma_{int} = 0.05$ and mechanical thermal occupation number $\bar{n}_{th} = 2$. Also, the initial mechanical mode has an occupation number of 0.5 , instead of being in its ground state, to give an example of a possible non-ground-state initial condition.

With these more realistic parameter values, the maximum detectable cat state has $\alpha_0 = 3$, with a squared separation of $S = |2\alpha_0^2| = 36$. This demonstrates that to store a mechanical cat state having $S = 100$, as has been generated experimentally in a microwave mode, will require reductions in the loss rates and mechanical reservoir temperatures compared to currently achieved values.

The ratio between the external cavity decay rate Γ_{ext} and the total cavity decay rate Γ_o has been quoted as the efficiency of an optomechanical state transfer protocol [33]. In our case, $\Gamma_{ext}/\Gamma_o = 0.95$, and we note that this only quantifies the amplitude being stored; the coherent quantum superposition in the quantum state has to be stored too. A quantum memory that has high amplitude efficiency, while retaining the quantum superposition of the stored quantum state is a challenge. The detection inefficiency which is not included in our model will no doubt make the verification of nonclassical quantum states even more difficult [93]. However, with the improvement in technologies such as optomechanical cooling using squeezed states [94], efficient quantum state transfer [26, 37] and detection schemes, the generation and verification of optomechanical cat states becomes feasible.

VI. CONCLUSION

In summary, we analyze a protocol for optomechanical storage of a Schrödinger cat state. To analyze its properties, a simplified decoherence model for a stored cat state was investigated by solving the single-mode master equation analytically. Additionally, the full coupled system including input and output was simulated using the positive-P phase space method. Provided importance sampling is utilized, this provides a compact and efficient probabilistic representation of such macroscopic quantum superpositions. The method allows straightforward quantum state sampling to be carried out, even for these

highly nonclassical, entangled multimode transients.

We then discussed typical cat state signatures as a measure of the quality of the quantum memory, and described the numerical methods required to compute these cat state signatures. The analytical predictions of the simplified model were then compared with our numerical results, showing good agreement. With the advent of finer quantum controls and manipulations in optomechanics and their physical implementations in different systems, the goal of creating and storing a small optomechanical cat state does appear achievable. We have investigated a number of different sources of decoherence, including losses in the optical system, losses in the mechanical system, initial thermal occupation of the mechanical oscillator, and finite temperature mechanical reservoirs. All of these clearly play a role in reducing the cat-state signatures, especially as the stored photon number is increased, but are not an insuperable barrier.

Our numerical methods provide an efficient way to probe the feasibility of this protocol with realistic experimental parameters. We show that a moderate size Schrödinger cat state with $n \leq 9$ stored quanta and a phase-space squared separation of $S = 36$ appears feasible with present quantum technologies.

ACKNOWLEDGEMENTS

MDR acknowledges support from Australian Research Council Discovery Grant DP180102470. PDD and MDR thank the hospitality of the Institute for Atomic and Molecular Physics (ITAMP) at Harvard University, supported by the NSF.

APPENDIX

Decoherence of the cat state

A cat state is extremely sensitive to fluctuations and losses due to the interaction with its environment. Here, we assume a simple model of decoherence provided by a master equation that includes damping and thermal noise, in order to obtain an analytical solution for the time evolution of a cat state in a simple *gedankenexperiment*. The time it takes for the Wigner function of a cat state to become positive is also investigated. This gives analytical insight and provides a comparison for the numerical results of the main text, which compute the final readout cat-state after a storage time in a quantum memory.

The time evolution of a single-mode density operator due to its interaction with a lossy environment is given by the following master equation:

$$\begin{aligned} \frac{\partial}{\partial t} \hat{\rho} = & \gamma \bar{n} (2a^\dagger \hat{\rho} a - a a^\dagger \hat{\rho} - \hat{\rho} a a^\dagger) \\ & + \gamma (\bar{n} + 1) (2a \hat{\rho} a^\dagger - a^\dagger a \hat{\rho} - \hat{\rho} a^\dagger a). \end{aligned} \quad (6.1)$$

Here, $\hat{\rho}$ is the cat state density operator, γ is the decay rate of the relevant mode and \bar{n} is the average thermal occupation number due to the interaction with the environment. Using phase space methods, we transform the above master equation into a time evolution equation of an s -ordered characteristic function. The advantage of using phase space methods is that the corresponding equations are much easier to solve than the operator equation Eq. (6.1). Here, the s -ordered characteristic function is based on the definition by Cahill and Glauber [95] and is given by

$$\chi_s(\lambda) = \text{Tr} \left[\hat{\rho} e^{\lambda \hat{a}^\dagger - \lambda^* \hat{a} + s |\lambda|^2 / 2} \right], \quad (6.2)$$

such that $s = -1, 0, 1$ corresponds to the characteristic function in Q, Wigner and P representations, respectively. By multiplying both sides of the Eq. (6.1) by $e^{\lambda \hat{a}^\dagger} e^{-\lambda^* \hat{a}}$ and taking the trace, it can be shown that the s -ordered characteristic function satisfies the following time evolution equation [96]:

$$\begin{aligned} \frac{\partial}{\partial t} \chi_s(\lambda, t) = & -\gamma \left(\lambda \frac{\partial}{\partial \lambda} + \lambda^* \frac{\partial}{\partial \lambda^*} \right) \chi_s \\ & - \gamma [s - (2\bar{n} + 1)] |\lambda|^2 \chi_s. \end{aligned} \quad (6.3)$$

Eq. (6.3) can be solved analytically using the method of characteristics. These analytical solutions allow us to compare with the numerical solutions obtained from a full quantum simulation in later sections.

Since characteristic functions of different order are related, we may choose $\bar{s} = 2\bar{n} + 1$ to simplify the partial differential equation Eq. (6.3). The corresponding partial differential equation is

$$\frac{\partial}{\partial t} \chi_{\bar{s}}(\lambda, t) = -\gamma \left(\lambda \frac{\partial}{\partial \lambda} + \lambda^* \frac{\partial}{\partial \lambda^*} \right) \chi_{\bar{s}} \quad (6.4)$$

and the solution can be shown to be [96]

$$\chi_{\bar{s}}(\lambda, t) = \chi_{\bar{s}}(\lambda e^{-\gamma t}, 0). \quad (6.5)$$

The s -ordered characteristic function at time t is then obtained through the relation

$$\chi_s(\lambda) = \exp \left\{ -[\bar{s} - s] \frac{|\lambda|^2}{2} \right\} \chi_{\bar{s}}. \quad (6.6)$$

Using Eq. (6.6) and the solution of the characteristic function in Eq. (6.5), the solution of an s -ordered characteristic function at time t is given by

$$\begin{aligned} \chi_s(\lambda, t) = & \exp \left\{ -[\bar{s} - s] \frac{|\lambda|^2}{2} (1 - e^{-2\gamma t}) \right\} \\ & \times \chi_{\bar{s}}(\lambda e^{-\gamma t}, 0). \end{aligned} \quad (6.7)$$

Based on this solution of the master equation, we can now investigate the time it takes for a cat state to lose its coherence. In the formalism of density operators, this corresponds to the absence of off-diagonal elements in a density operator. The corresponding density operator then describes a statistical mixture of two coherent states.

In the following subsections, we first compute the time taken for the off-diagonal terms of a cat density operator to vanish, when expressed using a coherent state basis. Another way to characterize the nonclassicality of a cat state is the negativity of the Wigner function. We also derive the upper bound for the time it takes for the Wigner function of a cat state to become positive.

Density operator off-diagonal terms: zero temperature case

In this subsection, we consider the case where the environment is at zero temperature $T = 0$, so that the mean mechanical thermal occupation number $\bar{n}_{th} = 0$. In this limit, the decay of the cat-state quantum coherence is due to the finite quantum memory decay rate. This allows us to gain insight on the rate of cat-state decoherence. The normally ordered characteristic function for the cat density operator (3.1), $\chi_1(\lambda)$, is a sum of four terms:

$$\chi_1(\lambda) = \frac{1}{\mathcal{N}} \left[e^{\lambda\alpha_0^*} e^{-\lambda^*\alpha_0} + e^{-\lambda\alpha_0^*} e^{\lambda^*\alpha_0} + \langle -\alpha_0 | \alpha_0 \rangle e^{-\lambda\alpha_0^*} e^{-\lambda^*\alpha_0} + \langle \alpha_0 | -\alpha_0 \rangle e^{\lambda\alpha_0^*} e^{\lambda^*\alpha_0} \right]. \quad (6.8)$$

Here, the first two terms correspond to the diagonal elements of the cat density operator and the last two terms correspond to the off-diagonal terms.

Next, we obtain the expression for the characteristic function of a cat state at time t , $\chi_s(\lambda, t)$. From Eq. (6.7) and further setting $s = 1$ (which corresponds to the normally ordered characteristic function), we find an expression with four terms involving exponentials of α_0 , α_0^* and $|\alpha_0|^2$, together with time-dependent factors. We identify two terms as the diagonal terms in a density operator $|\alpha_0 e^{-\gamma t}\rangle\langle\alpha_0 e^{-\gamma t}|$ and $|- \alpha_0 e^{-\gamma t}\rangle\langle - \alpha_0 e^{-\gamma t}|$ respectively, and the other two terms correspond to the off-diagonal terms $|\alpha_0 e^{-\gamma t}\rangle\langle - \alpha_0 e^{-\gamma t}|$ and $|- \alpha_0 e^{-\gamma t}\rangle\langle\alpha_0 e^{-\gamma t}|$ respectively, with a time dependent coefficient $e^{-2|\alpha_0|^2(1-e^{-2\gamma t})}$. The resulting density operator is given by

$$\hat{\rho}_{cat}(t) = \frac{1}{\mathcal{N}} \left[|\alpha_0 e^{-\gamma t}\rangle\langle\alpha_0 e^{-\gamma t}| + | - \alpha_0 e^{-\gamma t}\rangle\langle - \alpha_0 e^{-\gamma t}| + e^{-2|\alpha_0|^2(1-e^{-2\gamma t})} |\alpha_0 e^{-\gamma t}\rangle\langle - \alpha_0 e^{-\gamma t}| + e^{-2|\alpha_0|^2(1-e^{-2\gamma t})} | - \alpha_0 e^{-\gamma t}\rangle\langle\alpha_0 e^{-\gamma t}| \right]. \quad (6.9)$$

The off-diagonal terms in Eq. (6.9) vanish in a shorter time for larger coherent amplitude α_0 and damping rate γ . We note that in the absence of thermal noise, the off-diagonal terms never completely vanish i.e. there is no ‘‘sudden death’’ effect of the type discussed in Ref. [63].

Negativity of the Wigner function: finite temperature case

Here, we derive the upper bound on the time it takes for the cat state Wigner function to become completely positive. In this subsection, we include the effect of thermal noise. This approach is based on the paper of Paavola et al. [63]. In that paper, the upper bound of the time for any P function to lose its negativity is obtained by calculating the condition for that initial P function to turn into a Q function, which is always positive. The upper bound t_p was found to be

$$t_p = \frac{1}{2\gamma} \ln \left(\frac{1}{\bar{n}_{th}} + 1 \right), \quad (6.10)$$

where \bar{n}_{th} is the mean mechanical thermal occupation number and γ is the decay rate of the system. Following the same method, we obtain the upper bound of the time for a cat Wigner function to lose its negativity.

The Wigner function at time t is given by:

$$\begin{aligned} W(\alpha, t) &= \int \chi_{-1}(\lambda, t) e^{|\lambda|^2/2} e^{\lambda^*\alpha} e^{-\lambda\alpha} \frac{d^2\lambda}{\pi^2} \\ &= \int \chi_{-1}(\lambda e^{-\gamma t}, 0) e^{q(t)|\lambda|^2 + \alpha(\lambda^* - \lambda)} \frac{d^2\lambda}{\pi^2}, \end{aligned} \quad (6.11)$$

where Eq. (6.7) is used in the second line, and $q(t) \equiv 1/2 - (1 + \bar{n}_{th})(1 - e^{-2\gamma t})$.

The right side of the equation above will correspond to a Q function, which is always positive, if the condition $q(t) = 0$. The upper bound for the time it takes for the Wigner function of the cat state to be positive t_+ is therefore

$$t_+ = \frac{1}{2\gamma} \ln \left(\frac{1 + \bar{n}_{th}}{\frac{1}{2} + \bar{n}_{th}} \right). \quad (6.12)$$

Note that t_+ is not the time where a cat Wigner function is always positive, but the *upper bound* for the time it takes for a cat Wigner function to become positive. It is a function of the damping rate and the expectation value of the thermal occupation number, and is not a function of the size of the cat state.

To this end, it is worth noting that a non-negative Wigner function does *not* imply there is no cat-state quantum coherence. The numerical results for other cat-state signatures calculated at the time corresponding to t_+ are given in Section IV. At the time t_+ , while the Wigner negativity is zero, other signatures can indicate the presence of a cat-state. Let us focus on the density operator in Eq. (6.9) at the time t_+ for $\bar{n}_{th} = 0$. At the time $t_+ = 1/2\gamma \ln 2$, the off-diagonal terms in the density operator Eq. (6.9) do *not* vanish, albeit they make a tiny contribution that scales with the cat state amplitude as $\exp(-|\alpha_0|^2)$. This suggests that more than one signature should be measured and calculated in an experiment to conclusively verify the existence of a cat state.

- [1] E. Schrödinger, *Naturwissenschaften* **23**, 823 (1935).
- [2] S. Haroche, *Rev. Mod. Phys.* **85**, 1083 (2013).
- [3] D. J. Wineland, *Rev. Mod. Phys.* **85**, 1103 (2013).
- [4] M. Arndt and K. Hornberger, *Nature Physics* **10**, 271 (2014).
- [5] P. T. Cochrane, G. J. Milburn, and W. J. Munro, *Phys. Rev. A* **59**, 2631 (1999).
- [6] M. C. de Oliveira and W. J. Munro, *Phys. Rev. A* **61**, 042309 (2000).
- [7] O. P. de Sá Neto and M. C. de Oliveira, *Journal of Physics B: Atomic, Molecular and Optical Physics* **45**, 185505 (2012).
- [8] S. J. van Enk and O. Hirota, *Phys. Rev. A* **64**, 022313 (2001).
- [9] N. A. Ansari, L. Di Fiore, M. A. Man'ko, V. I. Man'ko, S. Solimeno, and F. Zaccaria, *Phys. Rev. A* **49**, 2151 (1994).
- [10] J. Joo, W. J. Munro, and T. P. Spiller, *Phys. Rev. Lett.* **107**, 083601 (2011).
- [11] D. S. Simon, G. Jaeger, and A. V. Sergienko, *Phys. Rev. A* **89**, 012315 (2014).
- [12] A. Ourjoumtsev, R. Tualle-Brouri, J. Laurat, and P. Grangier, *Science* **312**, 83 (2006).
- [13] J. S. Neergaard-Nielsen, B. M. Nielsen, C. Hettich, K. Mølmer, and E. S. Polzik, *Phys. Rev. Lett.* **97**, 083604 (2006).
- [14] K. Wakui, H. Takahashi, A. Furusawa, and M. Sasaki, *Opt. Express* **15**, 3568 (2007).
- [15] A. Ourjoumtsev, H. Jeong, R. Tualle-Brouri, and P. Grangier, *Nature* **448**, 784 (2007).
- [16] S. Deléglise, I. Dotsenko, C. Sayrin, J. Bernu, M. Brune, J.-M. Raimond, and S. Haroche, *Nature* **455**, 510 (2008).
- [17] H. Takahashi, K. Wakui, S. Suzuki, M. Takeoka, K. Hayasaka, A. Furusawa, and M. Sasaki, *Phys. Rev. Lett.* **101**, 233605 (2008).
- [18] A. Ourjoumtsev, F. Ferreyrol, R. Tualle-Brouri, and P. Grangier, *Nature Physics* **5**, 189 (2009).
- [19] T. Gerrits, S. Glancy, T. S. Clement, B. Calkins, A. E. Lita, A. J. Miller, A. L. Migdall, S. W. Nam, R. P. Mirin, and E. Knill, *Phys. Rev. A* **82**, 031802 (2010).
- [20] E. Bimbard, N. Jain, A. MacRae, and A. I. Lvovsky, *Nature Photonics* **4**, 243 (2010).
- [21] M. Yukawa, K. Miyata, T. Mizuta, H. Yonezawa, P. Marek, R. Filip, and A. Furusawa, *Opt. Express* **21**, 5529 (2013).
- [22] R. Dong, A. Tipsmark, A. Laghaout, L. A. Krivitsky, M. Ježek, and U. L. Andersen, *J. Opt. Soc. Am. B* **31**, 1192 (2014).
- [23] J. Etesse, M. Bouillard, B. Kanseri, and R. Tualle-Brouri, *Phys. Rev. Lett.* **114**, 193602 (2015).
- [24] K. Huang, H. Le Jeannic, J. Ruaudel, V. B. Verma, M. D. Shaw, F. Marsili, S. W. Nam, E. Wu, H. Zeng, Y.-C. Jeong, R. Filip, O. Morin, and J. Laurat, *Phys. Rev. Lett.* **115**, 023602 (2015).
- [25] A. E. Ulanov, I. A. Fedorov, D. Sychev, P. Grangier, and A. I. Lvovsky, *Nature Communications* **7**, 11925 (2016).
- [26] C. Wang, Y. Y. Gao, P. Reinhold, R. W. Heeres, N. Ofek, K. Chou, C. Axline, M. Reagor, J. Blumoff, K. M. Sliwa, L. Frunzio, S. M. Girvin, L. Jiang, M. Mirrahimi, M. H. Devoret, and R. J. Schoelkopf, *Science* **352**, 1087 (2016).
- [27] B. Vlastakis, G. Kirchmair, Z. Leghtas, S. E. Nigg, L. Frunzio, S. M. Girvin, M. Mirrahimi, M. H. Devoret, and R. J. Schoelkopf, *Science* **342**, 607 (2013).
- [28] J. I. Cirac, P. Zoller, H. J. Kimble, and H. Mabuchi, *Phys. Rev. Lett.* **78**, 3221 (1997).
- [29] H. J. Kimble, *Nature* **453**, 1023 (2008).
- [30] S. Ritter, C. Nölleke, C. Hahn, A. Reiserer, A. Neuzner, M. Uphoff, M. Mücke, E. Figueroa, J. Bochmann, and G. Rempe, *Nature* **484**, 195 (2012).
- [31] L. M. Duan, M. D. Lukin, J. I. Cirac, and P. Zoller, *Nature* **414**, 413 (2001).
- [32] Q. Y. He, M. D. Reid, E. Giacobino, J. Cviklinski, and P. D. Drummond, *Phys. Rev. A* **79**, 022310 (2009).
- [33] T. Palomaki, J. Harlow, J. Teufel, R. Simmonds, and K. Lehnert, *Nature* **495**, 210 (2013).
- [34] A. Schliesser, R. Rivière, G. Anetsberger, O. Arcizet, and T. J. Kippenberg, *Nature Physics* **4**, 415 (2008).
- [35] J. Teufel, T. Donner, D. Li, J. Harlow, M. Allman, K. Cicak, A. Sirois, J. D. Whittaker, K. Lehnert, and R. W. Simmonds, *Nature* **475**, 359 (2011).
- [36] J. Chan, T. M. Alegre, A. H. Safavi-Naeini, J. T. Hill, A. Krause, S. Gröblacher, M. Aspelmeyer, and O. Painter, *Nature* **478**, 89 (2011).
- [37] A. P. Reed, K. H. Mayer, J. D. Teufel, L. D. Burkhardt, W. Pfaff, M. Reagor, L. Sletten, X. Ma, R. J. Schoelkopf, E. Knill, and K. W. Lehnert, *Nature Physics* **13**, 1163 (2017).
- [38] T. A. Palomaki, J. D. Teufel, R. W. Simmonds, and K. W. Lehnert, *Science* **342**, 710 (2013).
- [39] R. Riedinger, A. Wallucks, I. Marinković, C. Löschnauer, M. Aspelmeyer, S. Hong, and S. Gröblacher, *Nature* **556**, 473 (2018).
- [40] C. F. Ockeloen-Korppi, E. Damskägg, J. M. Pirkkalainen, M. Asjad, A. A. Clerk, F. Massel, M. J. Woolley, and M. A. Sillanpää, *Nature* **556**, 478 (2018).
- [41] U. B. Hoff, J. Kollath-Bönig, J. S. Neergaard-Nielsen, and U. L. Andersen, *Phys. Rev. Lett.* **117**, 143601 (2016).
- [42] K. E. Khosla, M. R. Vanner, N. Ares, and E. A. Laird, *Phys. Rev. X* **8**, 021052 (2018).
- [43] D. V. Sychev, A. E. Ulanov, A. A. Pushkina, M. W. Richards, I. A. Fedorov, and A. I. Lvovsky, *Nature Photonics* **11**, 379 (2017).
- [44] M. Ringbauer, T. J. Weinhold, L. A. Howard, A. G. White, and M. R. Vanner, *New Journal of Physics* **20**, 053042 (2018).
- [45] J. Clarke and M. R. Vanner, *Quantum Science and Technology* **4**, 014003 (2019).
- [46] Q. He, M. Reid, and P. Drummond, *Optics Express* **17**, 9662 (2009).
- [47] S. Kiesewetter, R. Y. Teh, P. D. Drummond, and M. D. Reid, *Phys. Rev. Lett.* **119**, 023601 (2017).
- [48] J. Zhang, K. Peng, and S. L. Braunstein, *Phys. Rev. A* **68**, 013808 (2003).
- [49] F. Khalili, S. Danilishin, H. Miao, H. Müller-Ebhardt, H. Yang, and Y. Chen, *Phys. Rev. Lett.* **105**, 070403 (2010).
- [50] A. H. Safavi-Naeini and O. Painter, *New Journal of Physics* **13**, 013017 (2011).
- [51] Y.-D. Wang and A. A. Clerk, *Phys. Rev. Lett.* **108**, 153603 (2012).
- [52] R. Y. Teh, S. Kiesewetter, M. D. Reid, and P. D. Drummond, *Phys. Rev. A* **96**, 013854 (2017).

- [53] P. Bertet, A. Auffeves, P. Maioli, S. Osnaghi, T. Meunier, M. Brune, J. M. Raimond, and S. Haroche, *Phys. Rev. Lett.* **89**, 200402 (2002).
- [54] E. G. Cavalcanti and M. D. Reid, *Phys. Rev. Lett.* **97**, 170405 (2006).
- [55] C. Marquardt, U. L. Andersen, G. Leuchs, Y. Takeno, M. Yukawa, H. Yonezawa, and A. Furusawa, *Phys. Rev. A* **76**, 030101 (2007).
- [56] E. G. Cavalcanti and M. D. Reid, *Phys. Rev. A* **77**, 062108 (2008).
- [57] F. Fröwis and W. Dür, *New Journal of Physics* **14**, 093039 (2012).
- [58] P. Sekatski, N. Sangouard, and N. Gisin, *Phys. Rev. A* **89**, 012116 (2014).
- [59] E. Oudot, P. Sekatski, F. Fröwis, N. Gisin, and N. Sangouard, *J. Opt. Soc. Am. B* **32**, 2190 (2015).
- [60] F. Fröwis, N. Sangouard, and N. Gisin, *Optics Communications* **337**, 2 (2015), macroscopic quantumness: theory and applications in optical sciences.
- [61] B. Opanchuk, L. Rosales-Zárate, R. Y. Teh, and M. D. Reid, *Phys. Rev. A* **94**, 062125 (2016).
- [62] F. Fröwis, P. Sekatski, and W. Dür, *Phys. Rev. Lett.* **116**, 090801 (2016).
- [63] J. Paavola, M. J. W. Hall, M. G. A. Paris, and S. Manciscalco, *Phys. Rev. A* **84**, 012121 (2011).
- [64] P. D. Drummond and C. W. Gardiner, *Journal of Physics A: Mathematical and General* **13**, 2353 (1980).
- [65] A. Pace, M. Collett, and D. Walls, *Physical Review A* **47**, 3173 (1993).
- [66] S. Mancini, V. Giovannetti, D. Vitali, and P. Tombesi, *Phys. Rev. Lett.* **88**, 120401 (2002).
- [67] V. Giovannetti, S. Mancini, and P. Tombesi, *EPL (Europhysics Letters)* **54**, 559 (2001).
- [68] S. Kiesewetter, Q. Y. He, P. D. Drummond, and M. D. Reid, *Phys. Rev. A* **90**, 043805 (2014).
- [69] H. Carmichael, *Statistical Methods in Quantum Optics 1: Master Equations and Fokker-Planck Equations*, Theoretical and Mathematical Physics (Springer Berlin Heidelberg, 2013).
- [70] M. Wolinsky and H. J. Carmichael, *Phys. Rev. Lett.* **60**, 1836 (1988).
- [71] M. Reid and L. Krippner, *Phys. Rev. A* **47**, 552 (1993).
- [72] L. Krippner, W. Munro, and M. Reid, *Phys. Rev. A* **50**, 4330 (1994).
- [73] C. W. Gardiner and M. J. Collett, *Phys. Rev. A* **31**, 3761 (1985).
- [74] S. G. Hofer, W. Wiczczyk, M. Aspelmeyer, and K. Hammerer, *Phys. Rev. A* **84**, 052327 (2011).
- [75] Q. Y. He and M. D. Reid, *Phys. Rev. A* **88**, 052121 (2013).
- [76] B. Yurke and D. Stoler, *Phys. Rev. Lett.* **57**, 13 (1986).
- [77] A. Kenfack and K. Życzkowski, *Journal of Optics B: Quantum and Semiclassical Optics* **6**, 396 (2004).
- [78] E. Wigner, *Phys. Rev.* **40**, 749 (1932).
- [79] M. Hillery, R. O’Connell, M. Scully, and E. Wigner, *Physics Reports* **106**, 121 (1984).
- [80] L. G. Lutterbach and L. Davidovich, *Phys. Rev. Lett.* **78**, 2547 (1997).
- [81] A. I. Lvovsky and M. G. Raymer, *Rev. Mod. Phys.* **81**, 299 (2009).
- [82] W. Pfaff, C. J. Axline, L. D. Burkhardt, U. Vool, P. Reinhold, L. Frunzio, L. Jiang, M. H. Devoret, and R. J. Schoelkopf, *Nature Physics* **13**, 882 (2017).
- [83] W. Asavanant, K. Nakashima, Y. Shiozawa, J.-I. Yoshikawa, and A. Furusawa, *Opt. Express* **25**, 32227 (2017).
- [84] C. Eichler, D. Bozyigit, and A. Wallraff, *Phys. Rev. A* **86**, 032106 (2012).
- [85] P. D. Drummond and S. Chaturvedi, *Physica Scripta* **91**, 073007 (2016).
- [86] R. J. Glauber, *Phys. Rev.* **130**, 2529 (1963).
- [87] R. J. Glauber, *Phys. Rev.* **131**, 2766 (1963).
- [88] A. Gilchrist, C. W. Gardiner, and P. D. Drummond, *Phys. Rev. A* **55**, 3014 (1997).
- [89] P. Deuar and P. D. Drummond, *Phys. Rev. A* **66**, 033812 (2002).
- [90] S. Kiesewetter, R. Polkinghorne, B. Opanchuk, and P. D. Drummond, *SoftwareX* **5**, 12 (2016).
- [91] P. Drummond and I. Mortimer, *Journal of Computational Physics* **93**, 144 (1991).
- [92] C. E. Shannon, *Proceedings of the IRE* **37**, 10 (1949).
- [93] M. Skotiniotis, W. Dür, and P. Sekatski, *Quantum* **1**, 34 (2017).
- [94] J. B. Clark, F. Lecocq, R. W. Simmonds, J. Aumentado, and J. D. Teufel, *Nature* **541**, 191 (2017).
- [95] K. E. Cahill and R. J. Glauber, *Phys. Rev.* **177**, 1882 (1969).
- [96] S. Barnett and P. Radmore, *Methods in Theoretical Quantum Optics* (Clarendon Press, Oxford, 1997).